Water Resources Research

RESEARCH ARTICLE
10.1029/2023WR035719

Isogeochemical Characterization of Mountain System Recharge Processes in the Sierra Nevada, California

Sandra Armengol[1], **Hoori Ajami**[1], **Juan S. Acero Triana**[1], **James O. Sickman**[1], **and Lucia Ortega**[2]

[1]Department of Environmental Sciences, University of California, Riverside, CA, USA, [2]International Atomic Energy Agency, Vienna, Austria

Key Points:

- A multi-tool isogeochemical approach differentiates among mountain recharge pathways
- Incorporating chemical reactions in the End-Member Mixing Analysis strongly improves mixing ratio calculation
- Mountain block recharge originating from the Sierra Nevada accounts for 31%–53% of recharge in the southern Central Valley

Supporting Information:

Supporting Information may be found in the online version of this article.

Correspondence to:

S. Armengol and H. Ajami,
sandra.armengol.vall@gmail.com;
hoori.ajami@ucr.edu

Citation:

Armengol, S., Ajami, H., Acero Triana, J. S., Sickman, J. O., & Ortega, L. (2024). Isogeochemical characterization of mountain system recharge processes in the Sierra Nevada, California. *Water Resources Research*, *60*, e2023WR035719. https://doi.org/10.1029/2023WR035719

Received 11 JUL 2023
Accepted 21 JUN 2024

Author Contributions:

Conceptualization: Sandra Armengol, Hoori Ajami, Juan S. Acero Triana
Data curation: Juan S. Acero Triana
Formal analysis: Sandra Armengol, Hoori Ajami, James O. Sickman
Funding acquisition: Hoori Ajami
Investigation: Hoori Ajami
Methodology: Sandra Armengol, Hoori Ajami
Project administration: Hoori Ajami
Software: Lucia Ortega
Supervision: Hoori Ajami
Validation: Sandra Armengol, Juan S. Acero Triana

Abstract Mountain System Recharge processes are significant natural recharge pathways in many arid and semi-arid mountainous regions. However, Mountain System Recharge processes are often poorly understood and characterized in hydrologic models. Mountains are the primary water supply source to valley aquifers via lateral groundwater flow from the mountain block (Mountain Block Recharge) and focused recharge from mountain streams contributing to focused Mountain Front Recharge at the piedmont zone. Here, we present a multi-tool isogeochemical approach to characterize mountain flow paths and Mountain System Recharge in the northern Tulare Basin, California. We used groundwater chemistry data to delineate hydrochemical facies and explain the chemical evolution of groundwater from the Sierra Nevada to the Central Valley aquifer. Stable isotopes and radiogenic groundwater tracers validated Mountain System Recharge processes by differentiating focused from diffuse recharge, and estimating apparent groundwater age, respectively. Novel application of End-Member Mixing Analysis using conservative chemical components revealed three Mountain System Recharge end-members: (a) evaporated Ca-HCO_3 water type associated with focused Mountain Front Recharge, (b) non-evaporated Ca-HCO_3 and Na-HCO_3 water types with short residence times associated with shallow Mountain Block Recharge, and (c) Na-HCO_3 groundwater type with long residence time associated with deep Mountain Block Recharge. We quantified the contribution of each Mountain System Recharge process to the valley aquifer by calculating mixing ratios. Our results show that deep Mountain Block Recharge is a significant recharge component, representing 31%–53% of the valley groundwater. Greater hydraulic connectivity between the Sierra Nevada and Central Valley has significant implications for parameterizing groundwater flow models. Our framework is useful for understanding Mountain System Recharge processes in other snow-dominated mountain watersheds.

1. Introduction

Seasonal snowpacks and glaciers supply water to more than 16% of the global population (Barnett et al., 2005), and 24% of lowland populations rely on runoff from mountainous watersheds (Viviroli et al., 2020). While the contribution of mountain watersheds to streamflow is well known (Viviroli et al., 2020), the mechanisms of groundwater recharge processes in high-elevation mountain ranges are poorly understood (Gleeson & Manning, 2008). Likewise, the degree of hydraulic connectivity between the mountains and valley-fill aquifers is still uncertain (De Vries & Simmers, 2002). Prolonged droughts and reduced snowpack in the western US have increased reliance on groundwater (Scanlon et al., 2005), causing overexploitation of major aquifers, for example, California's Central Valley aquifer. Projected increases in the frequency and intensity of droughts, warmer temperatures (Diffenbaugh et al., 2015; Seager et al., 2007), and snow-to-rain transition (Berghuijs et al., 2014) are expected to alter the magnitude and direction of recharge rates. However, our ability to accurately estimate recharge in mountain catchments is limited due to the complexity of recharge processes and lack of direct recharge observations (Ajami et al., 2011; Bales et al., 2006).

Various terminologies have been used to describe recharge processes in a mountain-valley aquifer system (Markovich et al., 2019). Conceptually, a mountain-valley aquifer system consists of two units: a mountain aquifer unit extending from headwaters to the piedmont zone where mountains intersect alluvial deposits (Welch & Allen, 2012), and a valley bottom aquifer unit with boundaries starting at the piedmont zone. We define five recharge pathways along the mountain-valley aquifer continuum (Figure 1). The two main recharge pathways recharging the mountain aquifer are diffuse and focused Mountain Aquifer Recharge (MAR). Diffuse MAR results from snowmelt and rainfall infiltration into the mountain block, and focused MAR is from streamflow

Writing – original draft:
Sandra Armengol, Hoori Ajami
Writing – review & editing:
Sandra Armengol, Hoori Ajami, Juan S. Acero Triana, James O. Sickman

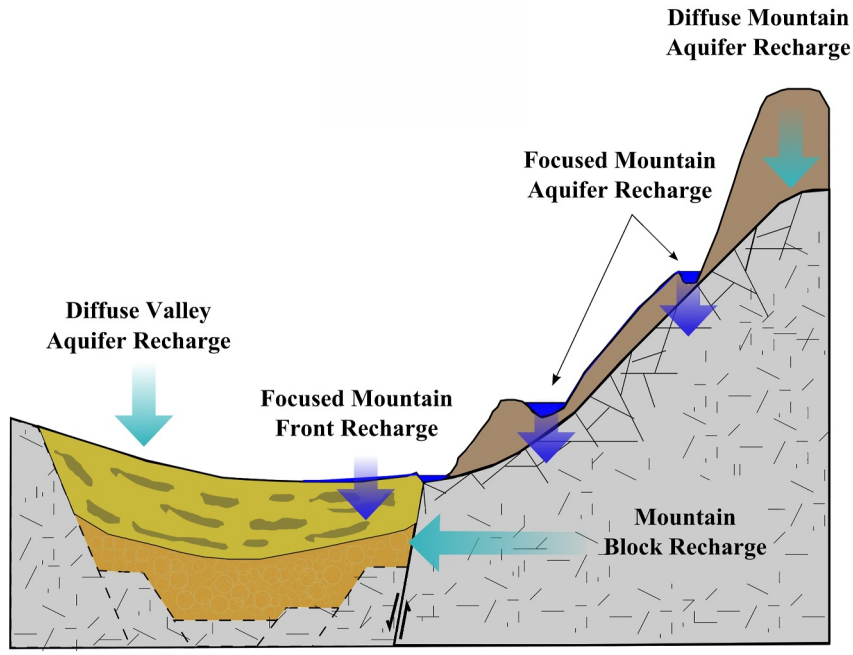

Figure 1. Conceptual illustration of five different recharge pathways in a mountain-valley aquifer system. Diffuse recharge processes refer to the direct infiltration of precipitation (diffuse Mountain Aquifer Recharge [MAR]) and/or irrigation (diffuse Valley Aquifer Recharge). Focused recharge processes refer to infiltration from streamflow or lakes. Mountain System Recharge includes diffuse and focused MAR, Mountain Block Recharge, and focused Mountain Front Recharge.

infiltration and seepage from lakes in the mountain block. The three main pathways recharging the valley aquifer are: diffuse Valley Aquifer Recharge due to precipitation and irrigation infiltration in the valley floor; focused Mountain Front Recharge because of streamflow infiltration in the piedmont zone; and Mountain Block Recharge as a result of subsurface flow from the mountain aquifer unit to the adjacent valley aquifer. Focused Mountain Front Recharge and Mountain Block Recharge may consist of different flow paths with distinct geochemical signatures and residence time (Bresciani et al., 2018; Frisbee et al., 2017). These four pathways, which originate from mountains and recharge the valley aquifer, are collectively called Mountain System Recharge.

Mountain Block Recharge and focused Mountain Front Recharge constitute significant recharge components in many arid and semi-arid aquifers (Wilson & Guan, 2004). Diffuse Valley Aquifer Recharge in arid and semi-arid aquifers is very small due to small precipitation and high evapotranspiration rates. Given differences in infiltration location and residence times of Mountain System Recharge pathways, it is essential to distinguish Mountain System Recharge pathways as they may respond differently to changes in hydroclimate and vegetation conditions (Markovich et al., 2019). While some hydrologists assumed that bedrock is impermeable, the application of geochemical tracers combined with heat and flow modeling demonstrated that Mountain Block Recharge contributes 5%–50% of total recharge (Aishlin & McNamara, 2011; Manning & Solomon, 2003; Markovich et al., 2019; Meixner et al., 2016). A recent synthesis of recharge from mountain aquifers showed that 61%–93% of MAR discharges via streams (Meixner et al., 2016) and eventually contribute to focused Mountain Front Recharge (Bazuhair & Wood, 1996; Coes et al., 2007; Goodrich et al., 2004; Schreiner-McGraw et al., 2019).

Various methods have been implemented to estimate Mountain System Recharge ranging from empirical relationships (e.g., Maxey & Eakin, 1949) to spatially distributed water balance models such as the Basin Characterization Model (Flint et al., 2004). Accurate Mountain System Recharge quantification requires characterizing the mountain aquifer unit and groundwater circulation depth (Frisbee et al., 2017), as well as the flow paths from the mountain block to the adjacent aquifers. Water balance models require a large amount of data typically unavailable in mountainous catchments due to extreme weather especially during winter, limited access due to complex terrain, and the presence of few mountain wells (Ajami et al., 2011; Tobin & Schwartz, 2016). Alternately, the chloride mass balance method (CMB) has been extensively used to estimate recharge rates in mountain catchments (Aishlin & McNamara, 2011). Chloride is considered a conservative solute as it is rarely

present in mountain bedrock and is neither evaporated nor transpired. Estimated annual Mountain System Recharge from the western Saudi Arabia mountains to arid alluvial aquifers using the CMB method was 3%–4% of mean annual precipitation in the valley (Bazuhair & Wood, 1996). However, estimated error was 30%–50% due to short-term data set. In the Dry Creek watershed in Idaho, CMB results showed that 14% of annual precipitation contributes to Mountain Block Recharge, and this contribution increases to 44% in the headwater areas (Aishlin & McNamara, 2011). Annual Mountain Block Recharge estimates from the Yucca Mountain in Nevada and Black Mesa in Arizona were 3%–5% and 3%–7% of mean annual precipitation, respectively (Zhu et al., 2003). Application of the CMB method in recharge studies is challenging as chloride retention in soils is not well understood (Shaw et al., 2014), and in low electrical conductivity environments such as snow-dominated mountains, chloride is not entirely conservative (Shaw et al., 2014). Furthermore, the CMB method typically accounts for a single tracer, and more than one tracer is usually needed to describe mixing dynamics and chloride equilibrium conditions in complex mountain-valley systems (Bresciani et al., 2018; Guan et al., 2013).

Christophersen and Hooper (1992) and Hooper et al. (1990) combined multiple tracers using a multivariate statistical analysis method (End-Member Mixing Analysis [EMMA]) to identify water sources in streamflow. The application of EMMA has been instrumental in identifying Mountain System Recharge sources (e.g., Wahi et al., 2008) and its partitioning. Wahi et al. (2008) applied a mixing model using isotopic ratios of oxygen ($\delta^{18}O$) and hydrogen ($\delta^{2}H$) in water in the Upper San Pedro River Basin, Arizona, attributing 70% of the Mountain System Recharge to winter and 30% to summer precipitation. Peng et al. (2018) applied EMMA to oxygen and hydrogen groundwater isotopes and electrical conductivity data from three alluvial fans in eastern Taiwan. They attributed 70% of the recharge to focused Mountain Front Recharge and Mountain Block Recharge and the remainder to diffuse Valley Aquifer Recharge. They showed that Mountain Block Recharge is mainly controlled by the degree of mountain bedrock fracturing, while the focused Mountain Front Recharge is impacted by streambed permeability and slope. Liu and Yamanaka (2012) applied EMMA to oxygen and hydrogen groundwater isotopes and major dissolved solutes and identified distance from the river and topography as important factors controlling focused Mountain Front Recharge. Frisbee et al. (2011) applied EMMA to electrical conductivity, calcium, magnesium, potassium, silica, and $\delta^{18}O$ and $\delta^{2}H$ of groundwater in two mountain watersheds in the Southwestern United States. They determined a deep circulation flow depth of 1–1.5 km depth, controlling stream chemistry and flow dynamics across the watershed.

Although EMMA has been successfully implemented in many studies, its application depends on selecting conservative tracers (Barthold et al., 2011; Carrera et al., 2004; Christophersen & Hooper, 1992; Hooper, 2003). Choosing conservative tracers is often challenging, mainly due to water-rock reactions and anthropogenic pollution affecting groundwater chemistry (Carrera et al., 2004; Parkhurst, 1997). The non-conservative behavior of species significantly decreases data set size, reducing the representativeness of the groundwater system (Rueedi et al., 2005). To broaden the application of EMMA using non-conservative tracers, Pelizardi et al. (2017) combined non-conservative solutes to create conservative chemical components. The conservative components were created by defining the chemical system in a stoichiometric matrix, *S*. The *S* matrix contains the reactions, the species, and the stoichiometric coefficients. The Mixing ratio calculation (MIX) program (Carrera et al., 2004) was run jointly with EMMA to estimate mixing ratios using conservative species concentration, while considering uncertainty in end-member concentrations using a maximum likelihood method. Goyetche et al. (2022) applied the Pelizardi et al. (2017) methodology to a coastal aquifer by using two conservative components. Conservative components accounted for cation exchange (CE) and mineral dissolution and redox reactions. Their results showed that 97% of the total variance was explained by the model considering conservative components.

In the California Central Valley aquifer system, Sierra Nevada snowpack contributes to 73% of total runoff (D. Li et al., 2017). Estimated groundwater recharge from the Central Valley hydrologic model indicates that Mountain System Recharge from the Sierra Nevada constitutes a significant natural recharge component, 20% compared to 11% from diffuse Valley Aquifer Recharge due to precipitation. Irrigation recharge accounts for 69% of the total recharge (Meixner et al., 2016). However, significant uncertainties exist in the Sierra Nevada's Mountain System Recharge estimates, and no information about groundwater flow paths from headwater catchments to the Central Valley aquifer system is available. These limitations are mainly due to the lack of borehole logs in the mountain aquifer, complex hydrogeologic setting of the Central Valley aquifer (Faunt et al., 2010), and spatiotemporal variability in precipitation and surface water deliveries that control irrigation demand, groundwater pumping and surface water-groundwater interaction (Scanlon et al., 2012). We aim to address this critical knowledge gap by using multiple tracers and EMMA to characterize regional groundwater flow paths from the southern Sierra

Nevada mountain aquifers to the northern Tulare Basin in California's Central Valley, and differentiate focused Mountain Front Recharge and Mountain Block Recharge processes. The Tulare Basin, located in the southern Central Valley, is one of the most overdrafted basins in California (Scanlon et al., 2012). Groundwater depletion in the Tulare Basin was 68% of the total groundwater loss in the Central Valley from 2006 to 2021 (Argus et al., 2022). Average groundwater depletion rate in the Central Valley was about 3 km^3/year over the last decades (Alam et al., 2019), and the depletion rate of the 2012–2016 drought (−10 km^3/year) was twice as high as that of the 2007–2009 drought (Xiao et al., 2017).

We used hydrochemical and isotope data from the US Geological Survey Groundwater Ambient Monitoring and Assessment (GAMA) program (Bennett et al., 2017) and implemented a multi-tool isogeochemical approach combined with EMMA and MIX analysis to answer three main research questions: (a) How does groundwater chemistry vary in the mountain-valley aquifer system of the northern Tulare Basin? (b) How to differentiate MAR, focused Mountain Front Recharge, and Mountain Block Recharge processes using major chemical solutes and isotope tracers? and (c) What is the hydraulic connectivity between the mountain and valley groundwater systems? These research questions correspond to the following three hypotheses:

1. Physical and chemical differences in the subsurface including variations in mineralogy, weathering rates of bedrock, and the presence of geological structures such as faults, within the mountain-valley aquifer system influence the spatial variability of groundwater chemistry, leading to distinct groundwater chemical facies along the mountain-valley aquifer continuum.
2. Isotopic fractionation and decay signatures in groundwater samples can differentiate Mountain System Recharge pathways by providing evidence to distinguish between rain and snow infiltration and surface water infiltration.
3. The permeability structure of the Sierra Nevada mountain block restricts the hydraulic connectivity between the mountain and valley aquifers, reducing the contribution of deeper subsurface flow paths from the mountain to the valley aquifer.

Given the complexity of flow paths and geochemical reactions in the mountain-valley aquifer system of the northern Tulare Basin, we only consider regional changes in groundwater chemistry. Local variability in hydrologic processes and their influence on groundwater chemistry is not fully accounted for in this study.

2. Materials and Methods

2.1. Study Area

The study area constitutes the northern Tulare Basin in California, with an area of 9,914 km^2 extending between the Coastal Range in the west and the Sierra Nevada in the east. The area encompasses the Kaweah River, Tule River, and Tulare Lake watersheds (Figure 2a). Historically, the Tule, Kaweah, and Kings Rivers discharged into the historical Tulare Lake. Elevation varies from 4,421 masl on Mount Whitney to below sea level in the valley, significantly impacting the climate. Lowlands (elevation <1,500 masl) and mid-elevation montane regions (1,500–2,500vmasl) have Mediterranean to semi-arid desert climate with hot and dry summers and cold winters (Boiano et al., 2005). Regions above 2,500 masl have Alpine climate with mean temperature lower than 10°C (Boiano et al., 2005). Mean annual precipitation varies between 150 mm in lowlands to over 1,000 mm at elevations above 2,500 m, and mainly occurs from November to March (Faunt et al., 2016; NOAA, 2022).

2.2. Geology and Hydrogeology

The physiography of the study region consists of the Sierra Nevada in the east, the Central Valley, and the faulted sedimentary, volcanic, and metamorphic rocks of the Coastal Range in the west (Lofgren & Klausing, 1969) (Figure 2b). The surface geology of the Sierra Nevada is dominated by Mesozoic granitic rocks (Figure S3 in Supporting Information S1), particularly biotite granodiorites (Sisson & Moore, 1984) composed of andesine ($Na_{.6}Ca_{.4}Al_{1.4}Si_{2.6}O_8$), and K-feldspar ($KAlSi_3O_8$) as well as quartz ($SiO_2$), and biotite ($KMg_3AlSi_3O_{10}(OH)_2$) (Clow et al., 1996; Feth et al., 1964; Garrels & Mackenzie, 1967; Sisson & Moore, 1984). Additionally, northwest-southeast bands of schists, quartzites, and marbles are reported along the mountain range derived from Mesozoic-aged marine sediments (Sisson & Moore, 1984). The marble bands are highly karstified (Tobin & Schwartz, 2012). The Central Valley sedimentary basin mainly consists of Tertiary marine to Quaternary continental sediments deposited over a crystalline pre-tertiary basement. Six central Tertiary to Quaternary

10.1029/2023WR035719

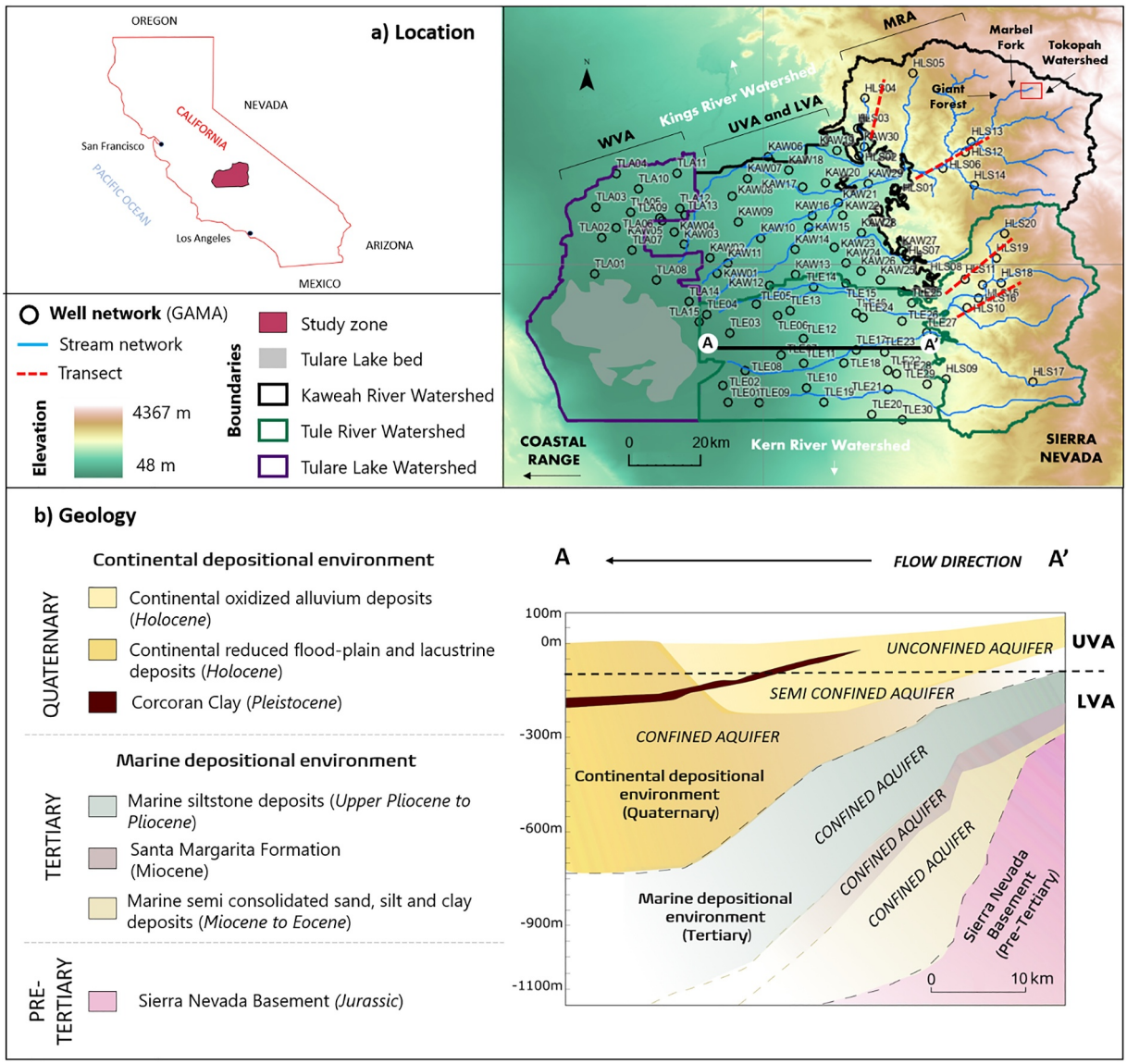

Figure 2. (a) Location of the study area comprising the Kaweah River, Tule River, and Tulare Lake watersheds, Ambient Monitoring and Assessment (GAMA) network, and four regions defined in this study: Mountain Range Aquifer (MRA), Upper Valley Aquifer (UVA), Lower Valley Aquifer (LVA) and Western Valley Aquifer (WVA). (b) Modified geologic cross section (A-A′) from Lofgren and Klausing (1969) with the main hydrogeological units. Vertical exaggeration is ×26.

sedimentary units are identified from bottom to top in the valley: (a) Marine semi-consolidated deposits (Tertiary), (b) the Santa Margarita Formation (Tertiary), (c) Marine siltstone deposits (Tertiary), (d) Lacustrine and flood-plain deposits (Quaternary), (e) Oxidized continental deposits (Quaternary), and (f) the Corcoran clay (Quaternary) (Figure 2b).

- The Marine semi-consolidated deposits with thicknesses between 60 and 460 m are Miocene to Eocene age marine sand, silt, and clay sequence (Hilton et al., 1963; Park & Weddle, 1959). These confined aquifers contain highly saline water (Lofgren & Klausing, 1969).
- The Santa Margarita Formation (Diepenbrock, 1933) is a Miocene age marine unit with 50–160 m thickness and mainly composed of fine gravel, fine to coarse sand, very fine green to gray clay, and shale facies (Hoots et al., 1954). This unit is the deepest freshwater aquifer in the study area used for agriculture (Lofgren & Klausing, 1969).

- The marine siltstone Pliocene and Pliocene deposits with 190–800 m thickness are siltstone diatomaceous deposits partially cemented by clayey siltstone interbedded with thin sand beds that contain saline water (Klausing & Lohman, 1964). The overall transmissivity of the siltstone unit is exceptionally low.
- The late Pliocene to Holocene reduced clay, silt, and sand green to gray lacustrine, and flood-plain deposits have maximum thicknesses of 1,000 m in the west (Davis et al., 1959; Frink & Kues, 1954; Inter-Agency Committee, 1958; Lofgren & Klausing, 1969). Plants and disseminated iron sulfide are well-preserved in them, and their saline water is not suitable for drinking or agricultural uses (Lofgren & Klausing, 1969).
- The Holocene oxidized continental alluvial deposits are yellow to brown highly weathered sand, silt, and sandy clay feldspar grains (Davis et al., 1959; Frink & Kues, 1954; Inter-Agency Committee, 1958; Lofgren & Klausing, 1969). The thickness of these highly weathered sediments is 90–200 m, and the unit is overlaid by 60–80 m of slightly weathered, highly calcareous permeable alluvial deposits. These calcareous deposits represent a time-lapse and a transition in the weathering regime (Lofgren & Klausing, 1969), constituting the principal aquifer in the study area.
- The Corcoran Clay deposits are silty clay to clayey silt diatomaceous Pleistocene deposits occupying half of the western side of the study area. These confining formations have thicknesses ranging from 0 m in the east to more than 30 m in the west (Lofgren & Klausing, 1969).

The regional groundwater flow is from east to west, following the Sierra Nevada streams. The oxidized alluvial deposits form the principal unconfined aquifer in the eastern part of the study area. In the west, the alluvial deposits are confined by the Corcoran Clay, forming semi-confined and confined aquifers. In the east, the saline water has naturally been replaced by fresh water forming a secondary confined aquifer in the Santa Margarita Formation. The low-quality high salinity groundwater is in the western part of the confined Pliocene sediments aquifer and the confined Santa Margarita Formation aquifer (Lofgren & Klausing, 1969).

2.3. Hydrochemical and Isotopic Data

We used hydrochemical and isotopic data from domestic wells sampled as part of the USGS GAMA Program (Bennett et al., 2017). The data set includes 95 wells sampled from November 2014 to April 2015. Among multiple groundwater-quality parameters, we used pH, temperature (T), alkalinity, major ions (Ca, Mg, Na, K, Cl, SO_4), SiO_2, NO_3, stable isotopic ratios of hydrogen (δ^2H) and oxygen ($\delta^{18}O$), carbon isotopes ($\delta^{13}C$ and ^{14}C), tritium (^3H) as well as noble gases (He, Ne, Ar, Kr, and Xe) in groundwater. The quality criterion for the chemical analyses was cation-anion imbalances of $\leq$10%. Only 40% of the wells (41) had ion imbalance errors smaller than 10% suitable for the chemical analysis. The remaining 54 wells were included for pH, temperature, δ^2H, $\delta^{18}O$, ^3H, $\delta^{13}C$, and ^{14}C, and noble gases analysis. Rainwater isotopic content was obtained from previous studies in California (Friedman et al., 1992; Rose et al., 1996; Visser et al., 2018). Meltwater isotopic signatures were obtained from a 2-year study in the Marble Fork of the Kaweah River watershed (Figure 2a) (Huth et al., 2004), indicating $\delta^{18}O$ ranges of -16 to $-14‰$ for the initial meltwater and -11 to $-10‰$ for the final meltwater (Huth et al., 2004).

The studied groundwater system was divided into four aquifer regions. The Mountain Range Aquifer (MRA) includes 18 wells at 181 to 876 masl with depths varying from 30 to 182 m. The Upper Valley Aquifer (UVA) comprises the unconfined regions of the Central Valley aquifer and includes 37 wells at elevations from 61 to 149 masl and depths of less than 100 m (17–98 m). The Lower Valley Aquifer (LVA) comprises the semi-confined to confined areas of the Central Valley aquifer and includes 23 wells with depths greater than 100 m (107–453 m) and elevations from 64 to 214 masl. The 100 m separation depth for differentiating the Upper and Lower Valley Aquifers was based on the geological cross-section A-A′ (Figures 2a and 2b) of Lofgren and Klausing (1969) and was confirmed by a recent large-scale geophysical investigation (Kang et al., 2022). This division was not applied to the 15 Western Valley Aquifer (WVA) wells close to the historical Tulare Lake. Elevation of these wells ranges from 66 to 81 masl, with depths from 24 to 91 m. Nearly all shallow wells pump fresh water from the continental oxidized alluvial deposits. Eastern LVA wells are pumping freshwater from saline Tertiary deposits, from which saline formation water has been flushed out and replaced with freshwater. Only wells in the WVA and western side of LVA are extracting water from the continental lacustrine deposits.

2.4. Isogeochemical Analysis and Modeling

2.4.1. Characterizing Chemical Facies of the Mountain-Valley Aquifer System

We employed a multi-tool approach using hydrochemical data to determine the chemical facies of aquifer regions. Groundwater chemical facies were determined by the Piper diagram and the spatial distribution of facies was determined by Stiff diagrams. The influence of soil-related processes on groundwater chemistry of the MRA was evaluated using three geochemical models run in PHREEQC version 3 (Parkhurst & Appelo, 2013). The plausibility of models was assessed by comparing the estimated dissolved cations concentrations with the average measured concentrations in the MRA. In the first model, evaporation was the main process driving dissolved cations concentrations. The evaporation effect was assessed by calculating a concentration factor (C_f) using the average evapotranspiration and rainfall rates for the 1982–2019 period (Elnashar et al., 2020; NOAA, 2022). The volume-weighted average rainwater composition of the Giant Forest station (Figure 2a) for the 1980–2020 period (NADP, 2022) was multiplied by the concentration factor to estimate average groundwater chemistry due to evapoconcentration. The second model included evaporation and CE processes. The average exchangeable base concentrations were obtained using soil information from two sites in the Tokopah watershed (Figure 2a). Exchange base concentration values were converted from meq/100 g to eq/kgw using sediment porosity of 0.45 and soil bulk density of 2.6 g/cm^3 (Table S6 in Supporting Information S1). The average exchange complex compositions were 0.02, 0.004, 0.003, and 0.002 eq/kgw for Ca-X_2, Mg-X_2, Na-X, and K-X, respectively. Exchange equilibrium constants were obtained from Appelo and Postma (2005) following the Gaines-Thomas convention (Equations 1–6).

$$Ca^{2+} + 2Na - X \leftrightarrow Ca{-}X_2 + 2Na^{+} \quad (1)$$

$$Ca^{2+} + 2K - X \leftrightarrow Ca - X_2 + 2K^{+} \quad (2)$$

$$Mg^{2+} + 2Na - X \leftrightarrow Mg - X_2 + 2Na^{+} \quad (3)$$

$$Mg^{2+} + 2K - X \leftrightarrow Mg - X_2 + 2K^{+} \quad (4)$$

$$CaCO_3 + H^{+2} \leftrightarrow Ca^{+2} + HCO_3^{-} \quad (5)$$

$$CO_{2(g)} + H_2O \leftrightarrow HCO_3^{-} + H^{+} \quad (6)$$

The third model considered evaporation, CE, and calcite dissolution until equilibrium using the averaged $pCO_{2(g)}$ of 2 bar in the MRA (Table S7).

While evaporation, CE and carbonate minerals dissolution are primarily soil-driven processes within the unsaturated zone, groundwater chemistry is highly influenced by other mineral dissolution-precipitation and mixing processes. These processes were evaluated using mineral saturation indices (SI), which indicate how far groundwater is from the mineral equilibrium and determine the dissolution or precipitation potential of a specific mineral. SI was computed with PHREEQC using groundwater temperature, pH, and alkalinity. Mineral equilibrium was assumed within ±0.5 of SI.

Complementary to the SI, bivariate analysis of groundwater dissolved solutes was performed to infer dissolution and precipitation processes that cannot be identified by the SI. For example, silicate dissolution is slow and silicate concentrations are expected to be far from equilibrium indicating sub-saturation. In addition, silicates are usually altered to other minerals with different chemical structure and composition. A well-known example is weathering of the Sierra Nevada granite silicates including andesine $Na_{0.62}Ca_{0.38}Al_{1.38}Si_{2.62}O_8$, K-feldspar and biotite $KMg_3AlSi_3O_{10}(OH)_2$ to kaolinite $Al_2Si_2O_3(OH)_4$, releasing Na, Ca, K, HCO_3 and SiO_2 as follows (Feth et al., 1964; Garrels & Mackenzie, 1967):

$$1.77\text{Andesine} + 2.44CO_2 + 3.67H_2O \rightarrow 1.23\text{Kaolinite} + 1.10Na^{+} + 0.68Ca^{2+} + 2.44HCO_3^{-} + 2.20SiO_2 \quad (7)$$

$$0.13\text{K} - \text{feldspar} + 0.13CO_2 + 0.195H_2O \rightarrow 0.065\text{Kaolinite} + 1.13K^{+} + 0.13HCO_3^{-} + 0.26SiO_2 \quad (8)$$

$$0.037\text{Biotite} + 0.51CO_2 + 0.26H_2O \rightarrow 0.037\text{Kaolinite} + 0.073K^{+} + 0.22Mg^{2+} + 0.51HCO_3^{-} + 0.15SiO_2 \quad (9)$$

Besides understanding water-rock reactions in the MRA, bivariate analysis was used to identify: (a) nitrate pollution from the agriculture fields through the NO_3-SO_4 relation, and (b) seawater mixing from the Tertiary marine deposits through the Na-Cl and SO_4-Cl relations in the Upper, Lower and Western Valley Aquifers.

2.4.2. Characterizing Mountain System Recharge Processes Using Stable Oxygen ($\delta^{18}O$) and Hydrogen ($\delta^{2}H$) Isotopes and Groundwater Age Tracers

Stable $\delta^{18}O$ and $\delta^{2}H$ isotopes of groundwater were used to identify recharge sources (rain, snowmelt, and surface water) and differentiate focused from diffuse MAR in the MRA wells. Stable $\delta^{18}O$ and $\delta^{2}H$ groundwater isotopes of 14 MRA wells in four transects across the elevation gradient (Figure 2a) were used in conjunction with isotopic values of rain and snowmelt from previous investigations to identify recharge sources. As focused MAR mainly occurs via streamflow infiltration and seepage from lakes through the mountain block, groundwater samples are expected to express isotopic fractionation due to evaporation compared to samples mainly recharged by diffuse MAR. Stable isotopic data from the evaporated MRA wells representative of focused MAR in the Sierra Nevada were used to build a Local Evaporation Line (LEL).

To differentiate focused Mountain Front Recharge and Mountain Block Recharge processes, stable $\delta^{18}O$ and $\delta^{2}H$ isotopes and groundwater age tracers were used. Shallow wells at the mountain front with the isotopic signature of evaporated Sierra Nevada rivers (focused MAR) and the chemical signature of unsaturated zone processes were attributed to focused Mountain Front Recharge. Deep wells with the chemical signature of water-granite reactions and long residence times were attributed to deep Mountain Block Recharge. It is essential to highlight that the depth of deep Mountain Block Recharge correlates with the maximum depth of deep sampling wells, which typically does not exceed 453 m in our study site. Mean groundwater apparent age was computed from dissolved tritium-helium (^{3}H-^{3}He) concentrations for samples with tritium concentrations greater than 0.5 tritium units (TU). For "tritium-dead" samples with an acceptable ion imbalance, ^{14}C of dissolved inorganic carbon along with a geochemical carbon mass-balance were used to estimate apparent groundwater age. A detailed description of ^{3}H-^{3}He and ^{14}C apparent age models are discussed in the Text S2 in Supporting Information S1.

2.4.3. End-Member Mixing Analysis (EMMA) and Mixing Ratio Calculations Using MIX

The proportion of focused Mountain Front Recharge and Mountain Block Recharge in the valley aquifer wells was computed using the (a) EMMA (Christophersen & Hooper, 1992; Hooper, 2003) and (b) MIX program (Carrera et al., 2004). EMMA is based on the principal component analysis, aiming to find the composition and a minimum number of end-members needed to explain the variability of measured concentrations within water samples. MIX calculates the mixing ratios of the identified end-members in each sample using the concentrations of conservative species while considering uncertainty in end-member concentrations. A detailed description of MIX can be found in Carrera et al. (2004), and a summary is provided below. The mass balance equation of a sample (mixture) p for species s is defined as (Carrera et al., 2004):

$$y_{ps} = \sum_{e-1}^{ne} \delta_{pe} x_{es} + \varepsilon_{ps} \quad \text{where } s = 1,\ldots,ns \tag{10}$$

where y_{ps} and x_{es} are the concentrations of species s in sample p and end-member e, respectively, δ_{pe} is the proportion of end-member e in mixture p, and ε_{ps} accounts for measurement and conceptual errors caused by the non-constant concentration of an end-member. MIX computes the mixing ratios by minimizing the residuals between the measured and estimated concentrations in each sample.

Correct application of EMMA and MIX requires selection of conservative species, and end-members with significant differences in species concentrations (Barthold et al., 2011; Carrera et al., 2004; Christophersen & Hooper, 1992; Hooper, 2003). As achieving conservative conditions due to water-rock reactions in groundwater is challenging (Carrera et al., 2004; Parkhurst, 1997), we followed the Pelizardi et al. (2017) approach by linearly combining non-conservative species with conservative chemical components. Components are linear combinations of species that remain unchanged by reactions. For example, the component $U_{\text{gypsum}} = Ca^{+2} - SO_4^{-2}$ will not change by gypsum dissolution (Equation 11), and the exact amount of Ca^{+2} and SO_4^{-2} release by gypsum dissolution is predicted by:

$$CaSO_{4(s)} \leftrightarrow Ca^{+2} + SO_4^{-2} \quad (11)$$

Therefore, subtracting the molar concentration of SO_4^{-2} from Ca^{+2} will always give the same result, maintaining U_{gypsum} constant. In order to build chemical components, the chemical reactions and species must be defined in a stoichiometric matrix (Equation 12), and components are built following Equation 13.

$$S = N_r \times N_s \quad (12)$$

$$U = (N_s - N_r) \times N_s \quad (13)$$

where S is the stoichiometric matrix containing the stoichiometric coefficients of the reactions, N_r is the number of reactions, N_s is the number of species, and U is a component. A detailed description of the component and stoichiometric matrices can be found in Molins et al. (2004) and Pelizardi et al. (2017), respectively. Components also helped validate processes identified in Section 3.1.1. In EMMA, eigenvectors indicate changes in species concentrations. Therefore, an eigenvector accounts for gypsum dissolution contributes the same amount to Ca^{+2} and SO_4^{-2} due to the stoichiometry of Equation 11. These contributions are in the same direction, either positive or negative, and range from 0 to 1. In general, more eigenvectors explain more variance of the sample composition as more species are considered.

In this study, end-members are defined to represent each main chemical groundwater type associated with Mountain System Recharge processes. A number of EMMA models were developed using different end-members, solutes, isotope tracers, and chemical reactions. The variance, coefficient of determination (R^2), root mean squared error (RMSE), and slope (m) of a linear regression between measured and estimated concentrations jointly determined the best model (i.e., the model with the highest variance and the best fit between measured and modeled concentrations). To account for the uncertainty in mixing ratio calculations, the best-performing EMMA model was run 100 times in MIX by considering uncertainties in measured concentrations. The top 5% of mixing models with the smallest differences between measured and estimated concentrations were selected to obtain the range of mixing ratios in each well. To quantify the degree of connectivity between the mountain and valley groundwater, regional averages of mixing ratios with its pooled standard deviation corresponding to each Mountain System Recharge process were calculated.

3. Results and Discussion

3.1. Characterizing Chemical Facies of the Mountain-Valley Aquifer System

The average groundwater temperature in all aquifer regions is 20°C, except for the LVA which is three degrees warmer (Figure 3c, Table S7). The average pH in the MRA is 7.0, and ranges from 7.6 to 8.0 in the Valley Aquifers (Figures 3c, Table S7). Overall, the Stiff and Piper diagrams indicate the presence of two major (Ca-HCO_3, Na-HCO_3) and three minor (Na-HCO_3SO_4, Na-Cl, Ca-Cl) chemical facies in the study area (Figures 3a and 3b). Ca-HCO_3 groundwater type dominates the Mountain Range and Upper Valley Aquifers, and Na-HCO_3 groundwater type dominates the Lower Valley and Western Valley Aquifers. Additionally, major solute analysis in 154 springs sampled during 2010–2012 at different elevations confirmed the prevalence of Ca-HCO_3-type over time in the MRA (Tobin, 2013). The presence of minor facies is due to higher concentrations of SO_4 and Cl relative to HCO_3 in some samples ($n = 11$). The Na-HCO_3SO_4 water type is present in the Western Valley and Lower Valley Aquifers ($n = 6$) (red circle in Figure 3b). The Cl-type chemical facies are presented by a few samples ($n = 5$) in the Valley Aquifers (blue circle in Figure 3b).

3.1.1. Processes Driving the Major Ion Evolution in the Mountain-Valley Aquifer System

3.1.1.1. Mountain Range Aquifer

To evaluate the influence of soil-related processes in the groundwater chemistry of the MRA, three models considering evaporation, CE, and calcite dissolution were developed (Table 1). Despite the importance of silicate weathering on the Sierra Nevada waters chemistry (Feth et al., 1964; Melack et al., 2020; Wahrhaftig & Birman, 1965; Williams et al., 1990, 1993), silicate weathering was not considered in these three models due to the kinetic behavior of silica minerals resulting in slow dissolution rate. Model A accounts for increases in dissolved

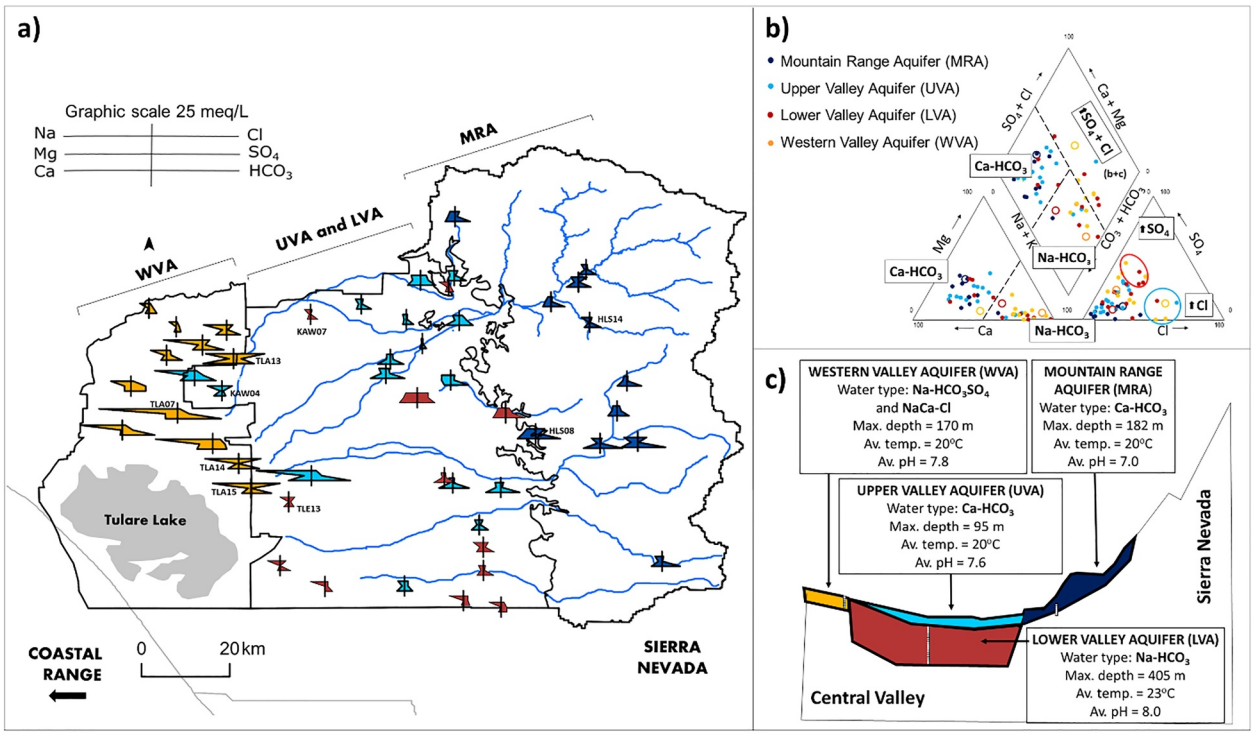

Figure 3. (a) Spatial distribution of the Stiff diagrams for each groundwater region: Mountain Range Aquifer (dark blue), Upper Valley Aquifer (light blue), Lower Valley Aquifer (red), Western Valley Aquifer (orange). (b) Projection of the major chemical component of groundwater samples on a Piper diagram. Red and blue polygons represent groundwater samples with higher dissolved SO_4 and Cl, respectively. Samples represented by empty circles are the selected end-members for calculating mixing ratios. (c) Main hydrochemical features of each groundwater region. Summary statistics are based on samples that met ≤10% cation-anion imbalances. Av. is average.

solutes due to evaporation. Considering the average evapotranspiration and rainfall rates of 639 and 756 mm/year, respectively (Elnashar et al., 2020; NOAA, 2022), 85% of precipitation is lost to evaporation in the MRA, resulting in a concentration factor of 5.45. As shown in Table 1, evaporation cannot solely explain cation concentrations in groundwater. Model B considers evaporation and CE processes. By incorporating these processes in Model B, estimated dissolved cations and Cl are less than 5% of the observed concentrations in the MRA. The underestimation of groundwater solutes in Model B can be attributed to the low solute concentration of rainwater and low CE capacity of the soils.

Including calcite dissolution in Model C, overestimates dissolved Ca by 109% and underestimates HCO_3 by 81% in the MRA. The feasibility of calcite dissolution is further supported by the SI of calcite in the MRA samples (Figure 4a), where most samples are equilibrated with this mineral. Tobin and Schwartz (2016) study of isolated small karst systems in the Sequoia National Park also reported that karst aquifers contribute to 65%–86% of

Table 1
Average Chemical Composition of the Volume-Weighted Average Rainfall at the Giant Forest Rain Station During the 1980–2020 Period (First Row), and Average Cation, Cl, and HCO_3 Concentrations in the Mountain Range Aquifer Region (mg/L)

	Ca	Mg	K	Na	Cl	HCO_3
Volume-weighted average Rainfall (1980–2020)	0.05	0.01	0.02	0.06	0.11	–
Average Mountain Range Aquifer concentration	60	16.8	4.2	39.1	34.3	273
Model A—Evaporation	0.27	0.05	0.11	0.33	0.60	–
Model B—Evaporation + CE	0.001	0.0001	0.19	0.63	0.60	–
Model C—Evaporation + CE + Calcite dissolution	65.5	0.59	0.02	0.34	0.60	221.7

Note. Calculated cation and Cl concentrations from Model A, B, and C by considering concentration by evaporation, cation exchange (CE) and calcite dissolution processes.

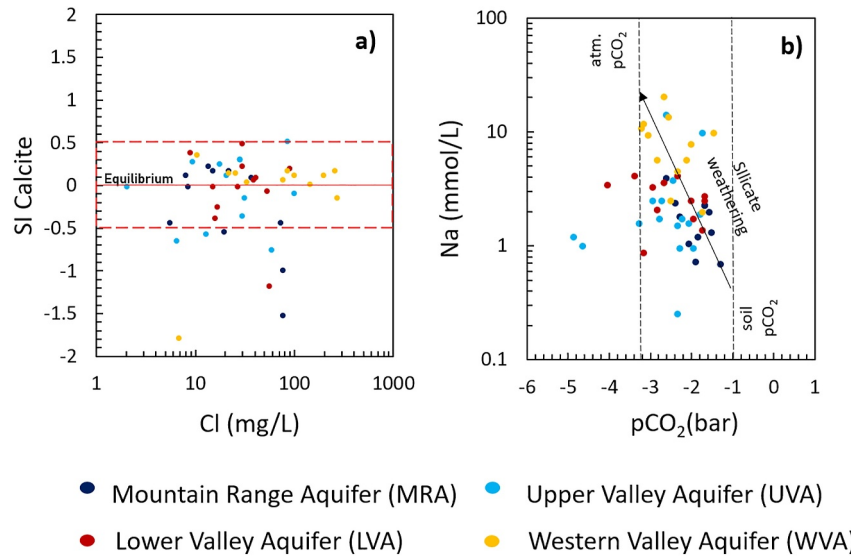

Figure 4. (a) Evolution of calcite saturation (saturation indices [SI] of calcite ($CaCO_3$)) with mineralization (dissolved Cl in mg/L). While most groundwater samples are equilibrated with respect to calcite, samples with SI < 0 indicate undersaturation. The degree of mineralization indicated by the total dissolved Cl (mg/L) is independent of calcite saturation. Low mineralized samples with saturated calcite could indicate calcite dissolution in the early recharge stages. (b) Increases in silicate weathering such as andesine (dissolved Na in mmol/L) reduces dissolved edaphic CO_2 (pCO_2 bar).

baseflow during the dry season in the North and East Fork of the Kaweah River, leading to significant increases in dissolved Ca due to calcite dissolution (Tobin & Schwartz, 2016).

Furthermore, past research has illustrated that Ca is released in part through the dissolution of calcite in Sierra Nevada waters (White et al., 1999), as observed in similar watersheds predominantly characterized by granitoid (Clow et al., 1997; Mast et al., 1990). Garrels and Mackenzie (1967) attributed 70% of Ca variability in the perennial springs of the Sierra Nevada to calcite dissolution and the remainder to silicate weathering.

While Models A, B, and C aim to qualitatively assess the influence of soil-related processes on MRA chemistry, several limitations exist. These models ignore the variability in groundwater chemistry, heterogeneities in soil type and CE capacity, and influence of processes such as road salt dissolution and granite weathering.

The feasibility of road salt dissolution from mountain roads was assessed by a semi-quantitative analysis and comparing Na and Cl concentrations in groundwater. Considering that salt is mainly NaCl and its dissolution could explain the remaining 34 mg of Cl (0.95 mmol) in groundwater after evaporation, road salts contribution to Na will be 22 mg of Na (equivalent to 0.95 mmol of Na), accounting for 56% of the total dissolved Na. This result suggests that road salt could contribute to a significant amount of dissolved Na and Cl in the MRA (Table 1). However, road salt application is prohibited in the higher elevation zones of the Kaweah River Watershed under the Sequoia National Park jurisdiction.

Silicate weathering was assessed for andesine and biotite, the most prevalent or rapidly weathering silicates in the Sierra Nevada (Clow et al., 1996; Feth et al., 1964; Garrels & Mackenzie, 1967; Sisson & Moore, 1984), via qualitative analysis of weathering products and comparison with the estimated Na, Mg, and K concentrations from Model C and road salt dissolution (Table 1). Figure 4b shows that Na increases with decreases in CO_2, most likely due to andesine weathering (Equation 7). Therefore, the remainder of dissolved Na in groundwater that could not be explained by Model C and road salt dissolution is likely caused by andesine weathering. Biotite is less prevalent than andesine but is the most easily weathered silicate in the Sierra Nevada (Meade, 1967; Wahrhaftig & Birman, 1965). Differences between the Model C estimated dissolved K and Mg and observed concentrations in groundwater could be explained by biotite weathering following Equation 9. Higher silica concentration in the MRA samples is consistent with silicate weathering (Table S7). Therefore, andesine and biotite weathering are likely the main sources of dissolved Na, Mg, and K, while Ca is from the karst system.

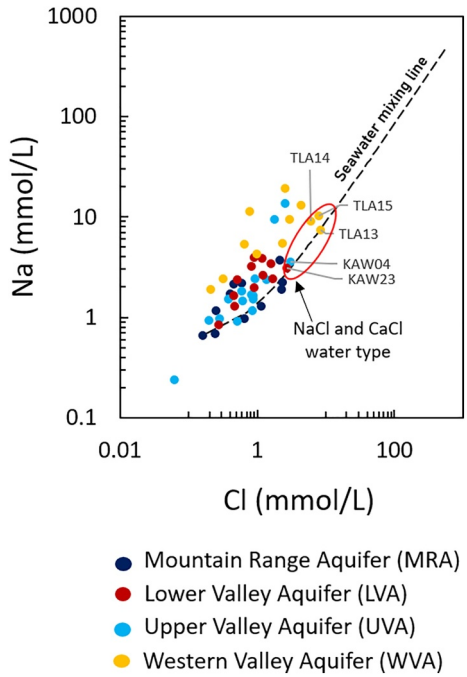

Figure 5. Results of the mixing model between freshwater and connate saline water samples indicate that dissolved Cl and Na concentrations of the Na-Cl-type and Ca-Cl-type samples are mainly due to seawater mixing. The presence of additional dissolved Na (mmol/L), along with the dominance of HCO_3 over Cl and low mineralization (Cl < 2.3 mmol/L) observed in most samples above the mixing line, suggest the absence of seawater mixing.

3.1.1.2. Valley Aquifer System

The valley area comprises the Upper Valley, Lower Valley, and Western Valley Aquifers. Diffuse recharge by precipitation is very low in this region, given the low precipitation (244 mm/year) (NOAA, 2022) and high evaporation rate (529 mm/year) (Elnashar et al., 2020). As a result, focused Mountain Front Recharge and Mountain Block Recharge processes after irrigation recharge are the main sources of recharge (Figure 1). According to the Stiff diagrams, the Ca-HCO_3 chemical facie originating from the MRA extends to the UVA, resulting in a shallow flow path with the Ca-HCO_3 signature. On the contrary, the LVA is Na-HCO_3-type. We attributed the Na-HCO_3-type to the prevalence of andesine ($Na_{.6}Ca_{.4}Al_{1.4}Si_{2.6}O_8$) after quartz in the Sierra Nevada biotite granodiorites, which promotes a slow but constant release of Na to the aqueous phase of a deeper flow path. This hypothesis is supported by the low mineralization of LVA samples (i.e., smaller Stiff diagrams in Figure 3a), and warmer temperature of the LVA associated with the geothermal characteristics of deep flow circulation (Figure 3c). Further support for shallow and deep flow paths is provided by computing the groundwater apparent age in Section 3.2.

The chemical composition of the WVA is similar to the LVA but more mineralized, with higher dissolved SO_4 and dominance of Cl over HCO_3 in some wells (Figure 3a). These properties were attributed to the influence of Miocene marine sedimentary rocks derived from the Coast Range (Fujii & Swain, 1995). Potential mixing of connate saline groundwater in marine sediments with freshwater was evaluated by developing a binary mixing model (Figure 5). The short distances of Na-Cl-type and Ca-Cl-type samples from the mixing line indicates that seawater mixing is the main contributor to dissolved Cl and Na in Cl-type samples. Note that the other two Cl-type samples from the Upper Valley and Lower Valley Aquifers are also affected by the seawater mixing. Source of SO_4 in the WVA is uncertain given subsaturation of samples and lack of sulfur isotopes. Therefore, gypsum dissolution is most likely responsible for releasing SO_4 in groundwater (Text S1 in Supporting Information S1).

3.2. Characterizing Mountain System Recharge Processes Using Stable Oxygen ($\delta^{18}O$) and Hydrogen ($\delta^{2}H$) Isotopes and Groundwater Age Tracers

Groundwater δ^2H and $\delta^{18}O$ values from all four aquifer regions are plotted along the Global Meteoric Water Line (GMWL; Craig, 1961) (Figure 6a). The isotopic content of the samples ranges from −51.1 to −97.4‰ for δ^2H and −5.68 to −13.59‰ for $\delta^{18}O$ (V-SMOW) (Figure 6a). A LEL was determined from the MRA samples (Figure 6a). To identify recharge sources, the isotopic composition of 14 samples along four elevation transects (Figure 6b) was used to assess the topographic fractionation effect in the study area. The slope of topographic fractionation effect in California ranges from −1.7 to −2.7‰ per vertical km for $\delta^{18}O$‰ (Friedman et al., 1992; Lechler & Niemi, 2012; Rose et al., 1996; Visser et al., 2018). The observed topographic fractionation effect between the $\delta^{18}O$ values of T1 and T4 wells (676 m altitude difference; Figure 6b), is 0.42‰ compared to the estimated topographic fractionation of 1.2–1.8‰. The difference between the observed and estimated fractionation is interpreted as a result of snowmelt fractionation controlling the isotopic composition of infiltration water. Therefore, the $\delta^{18}O$-$\delta^{2}H$ isotopic space was divided by the precipitation type considering different stages of snowmelt to identify recharge sources.

According to Figure 6a, isotopic values of MRA samples mostly follow the LEL ($\delta^{18}O$ values ranging from −9.82 to −5.68‰). Due to the lack of isotope data for soil water and streams in the study site, it is uncertain whether the evaporation signature, which agrees with the slope of the US rivers (Kendall & Coplen, 2001), is caused by the focused recharge or rain infiltration within the unsaturated zone of the upland areas. To evaluate this hypothesis, groundwater apparent age was computed using ^3H-^3He measurements for the MRA samples as tritium concentration is greater than 0.5 TU. Results indicate that groundwater samples that do not align with the LEL belong to higher elevation wells and are more depleted (mean $\delta^{18}O = -9.8$‰, $n = 8$), with a mean apparent age of

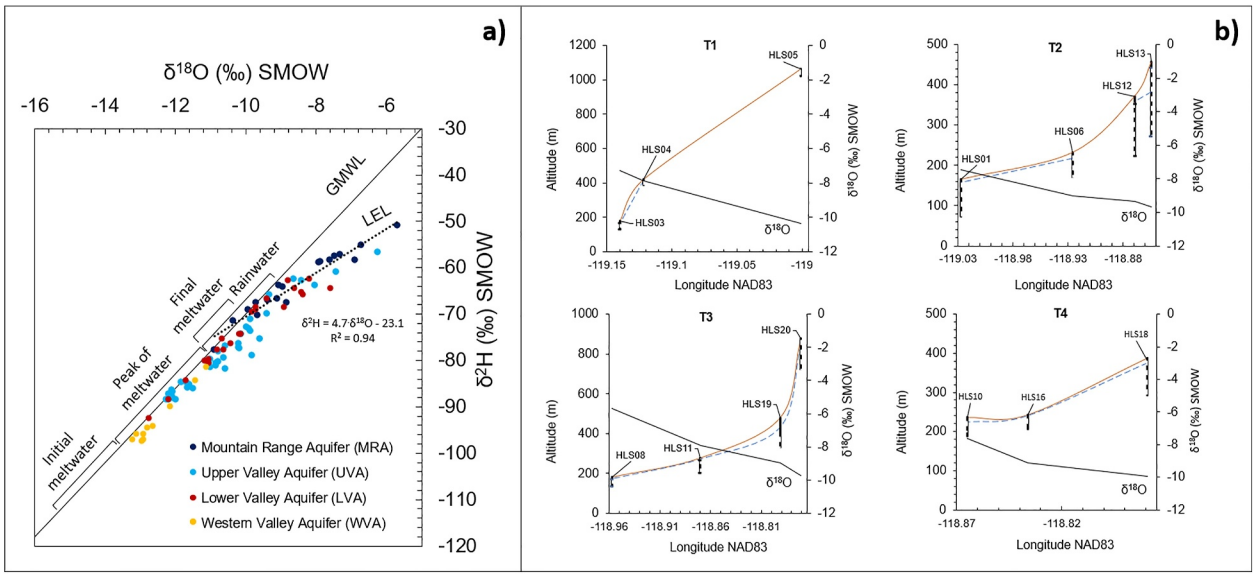

Figure 6. (a) δ^2H and $\delta^{18}O$ content in groundwater. Global Meteoric Water Line (GMWL; Craig, 1961) and Local Evaporation Line ($\delta^2H = 4.7\ \delta^{18}O$—23.3). Initial and final meltwater isotopic ranges are from Huth et al. (2004). Rain isotopic values are from Friedman et al. (1992), Rose et al. (1996), and Visser et al. (2018). (b) Variability of $\delta^{18}O$ values along four transects in the Mountain Range Aquifer are shown in relation to altitude of wells (orange line), groundwater level (discontinuous blue line), well depth (black line) and screen depth (discontinuous black line). Groundwater samples from higher altitudes are more depleted compared to the mountain front wells.

35.3 years ($n = 7$). These wells are relatively deep, with a mean depth of 98.7 m ($n = 8$), and have deeper groundwater levels (mean depth to groundwater level = 24.3 m, $n = 6$). Therefore, they were attributed to diffuse MAR.

On the other hand, MRA wells that are plotted along the LEL (Figure 6a) exhibit evaporation signature (mean $\delta^{18}O = -7.5‰$, $n = 10$), and are located at lower elevations (165–479 masl except for HLS17, 811 masl). These wells have shallower groundwater levels (mean depth to groundwater level = 12.8 m, $n = 10$) and a mean apparent age of 10.3 years ($n = 5$). Younger groundwater age in these wells where data are available indicates recharge through faster flow paths. If significant evaporation occurs during transient recharge in the unsaturated zone, correlations between $\delta^{18}O$ and both depth to groundwater level and groundwater age are expected. However, no correlations between depth to groundwater level and $\delta^{18}O$ (indicative of evaporation effect) were found, and the coefficient of determination between age and $\delta^{18}O$ is 0.45 ($n = 5$). By only including wells with shallower depth to groundwater level (<10 m, $n = 6$), the correlation between $\delta^{18}O$ and depth to groundwater level significantly improves ($R^2 = 0.74$), suggesting the influence of evaporation during infiltration at shallower groundwater level depths. However, only three out of six samples have age data, so no robust calculations can be made. The proximity of evaporated mountain aquifer wells to streams, lower mean annual precipitation (292–528 mm/year) (Daly et al., 1994), higher annual evapotranspiration (20-year average precipitation-evaporation is negative for 7 out of 10 wells), and a shift from forest to shrublands and grasslands (NLCD, 2019) at the locations of these evaporated groundwater samples further suggest the influence of focused MAR. In addition, the Ca-HCO_3 groundwater type of the MRA has been reported for most Sierra Nevada rivers and lakes (Melack et al., 1985, 2020; White et al., 1999). Although the role of local precipitation recharge cannot be ignored and is potentially important, additional data sets are needed to better understand recharge processes and separate the influence of focused MAR from diffuse recharge at lower elevation wells.

The UVA groundwater samples located at the mountain front or close to the Kaweah River also follow the LEL (KAW18,19,25,26,28,29; TLE23,25,27) (Figure 6a) and are Ca-HCO_3 type (Figure 3a). The evaporation signal of these Ca-HCO_3-type samples in the UVA is interpreted as focused MAR that progresses to focused Mountain Front Recharge in the piedmont zone.

The non-evaporated Ca-HCO_3–type of some UVA samples is interpreted as diffuse MAR that progresses to shallow Mountain Block Recharge recharging the first 100 m of the unconfined aquifer. The LVA groundwater

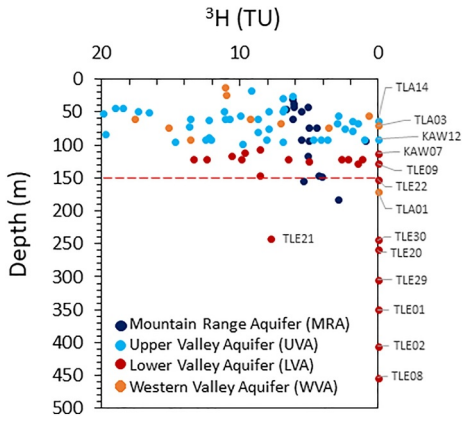

Figure 7. Tritium content (Tritium Units, TU) of groundwater samples with depth in the study region. The variability in tritium concentration at shallower depths (<150) indicates recent recharge and mixing with deeper flow paths due to pumping. The majority of deeper wells (>150 m) belong to tritium dead zones, corresponding to groundwater with an apparent age >50 years.

samples from the deeper wells (depth >150 m) close to the mountain front (TLE20, 22, 29, and 30; Figure 2a and Table S7) also follow the LEL and are mostly Na-HCO_3-type interpreted as focused MAR that evolves to deep Mountain Block Recharge. Non-evaporated LVA and all WVA samples following the GMWL are interpreted as recharged by diffuse MAR through meltwater infiltration during the peak of snowmelt (days 170–210 of the water year). Meltwater that flows through the saprolite, faults, and joints, eventually reaches the deeper aquifer (Na-HCO_3-type) and contributes to deep Mountain Block Recharge.

To further validate shallow and deep Mountain Block Recharge pathways in the Valley Aquifer, groundwater apparent age was computed using ^{3}H-^{3}He measurements for samples with more than 0.5 TU and ^{14}C measurements for samples with less than 0.5 TU (Text S2 in Supporting Information S1). While tritium content of more than 0.5 TU was reported in all Valley Aquifer regions, samples with less than 0.5 TU belong mostly to Lower and WVA wells with depths of more than 150 m (Figure 7). The resulting apparent ages of groundwater in the Valley Aquifer ranges from 3.7 to 102 years based on ^{3}H-^{3}He age to more than 40k years based on the ^{14}C apparent age results. The apparent age of UVA samples ranges from 3.7 ± 1 to 71 ± 4 years and agrees with focused Mountain Front Recharge and shallow Mountain Block Recharge processes through shorter flow paths. Lower Valley Aquifer samples with tritium belong to wells with depths less than 150 m (Figure 7). These wells have long screens, and the screen top is in the unconfined aquifer. The apparent age of these samples ranges from 15 ± 6 to 102 ± 7 years. Lower Valley Aquifer wells with "tritium-dead" samples are at depths greater than 150 m (Figure 7) and have an apparent age of 1.6k to more than 40k years consistent with the proposed deep Mountain Block Recharge. The younger apparent age of shallower wells in the LVA is likely caused by the mixing between the shallower flow path recharging the UVA and the deep flow path and cannot be solely attributed to the high focused Mountain Front recharge rate. This inference is consistent with the analyses of tritium data across the continental US indicating propagation of modern groundwater to deeper depths in intensively pumped aquifer systems (Thaw et al., 2022).

The apparent age of WVA samples is mixed. The apparent age of groundwater samples that contain tritium ranges from 7 ± 1 to 92 ± 14 years and agrees with a mixture of shallow and deep flow paths. However, the apparent age of "tritium-dead" samples is more than 12k years and agrees with recharge from deeper flow paths. Significant differences in groundwater age across the aquifer agree with the different recharge pathways summarized in Figure 8.

3.3. Determining Mountain Block Recharge and Focused Mountain Front Recharge Contributions via End-Member Mixing Analysis (EMMA)

3.3.1. End-Member and Solutes Selection for EMMA

Results of the chemical and isotopic analyses informed end-member selection. To explain the chemical variability of groundwater, different mixing models were developed to find the best end-members and tracers. These models included different combinations of end-members and tracers, and the model selection was based on the percentage of variance explained by the three eigenvectors (EG1, EG2, and EG3) while ensuring that the projected components were enclosed by the end-member triangle at the EG1–EG2 and EG1–EG3 projection space. For the end-member analysis, two general models with 3 and 4 end-members were developed (Table 2). Model 1 consists of an evaporated Ca-HCO_3 groundwater type sample (HLS08) from the MRA representing focused Mountain Front Recharge, a 0-Tritium Na-HCO_3 sample (KAW07) from the LVA to represent the deep Mountain Block Recharge, and a Na-HCO_3SO_4 groundwater type sample (TLA07) from the WVA representing deep Mountain Block Recharge with long exposure to water-rock reactions. In addition to end-members in Model 1, Model 2 includes a Ca-Cl groundwater sample (TLA13) from the WVA representing mixing with connate seawater. This sample is not related to the Mountain System Recharge processes. All selected end-members are plotted as empty circles in Figure 3b.

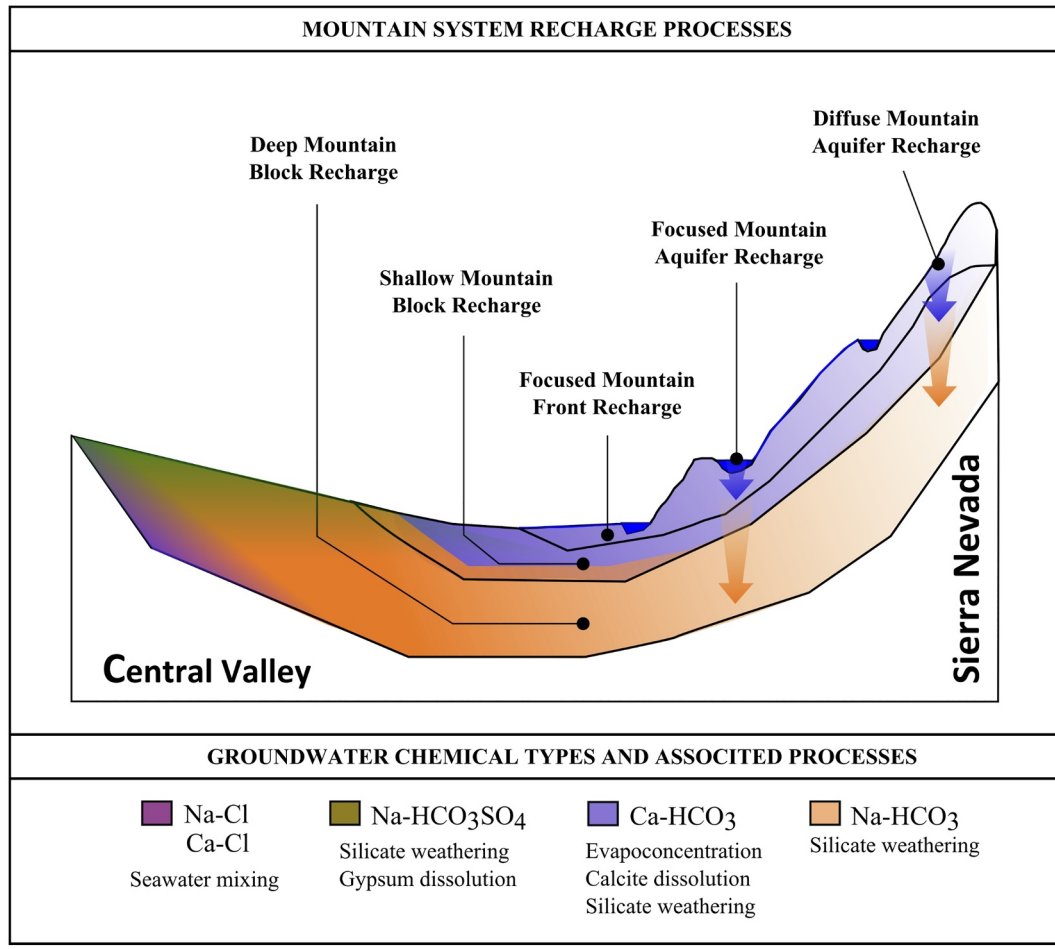

Figure 8. Conceptual illustration of the relation between the five recharge pathways in the study area, along with the main groundwater chemical types and their associated hydrogeochemical processes. Chemical groundwater facies are shown in different colors representing two major chemical facies such as Ca-HCO_3 and Na-HCO_3, and three minor chemical facies. Polygons represent the spatial distribution of focused Mountain Front Recharge, shallow Mountain Block Recharge, and deep Mountain Block Recharge.

In Model 1, the coefficient of determination between the measured and estimated values of Mg, K, and SO_4 is satisfactory ($R^2 \geq 0.75$; RMSE ≤ 0.32). However, poor results are obtained for Cl, Na, alkalinity (RMSE ≥ 1.75), Ca, and pH ($R^2 \leq 0.44$). Model 2 results are satisfactory for Mg, K, and pH ($R^2 \geq 0.77$; RMSE ≤ 0.39) and are significantly better than Model 1 for Ca and Cl ($R^2 \geq 0.72$; RMSE ≤ 0.6). However, further improvement in estimating Na, alkalinity (RMSE ≥ 1.71), and pH ($R^2 \leq 0.2$) is needed. Differences between measured and estimated concentrations are related to overestimation of all solutes, except SO_4 ($m < 1$; Table 2). Among all parameters in Model 2, pH is the only one with a non-acceptable R^2 (0.1; Table 2). This result suggests that multiple non-linear reactions affect pH.

To improve Model 2 performance, different tracers were added or removed, resulting in Model 2a to 2d (Table 2). Removing pH in Model 2a increased the total variance explained by all the solutes by 4% (Table 2). Stable $\delta^{18}O$ (‰), $\delta^{2}H$ (‰), and $\delta^{13}C$ (‰) isotopes were added in Models 2b, 2c, and 2d, respectively. However, very poor R^2 and RMSE were obtained, and the total explained variance decreased to 79%. EMMA seems inappropriate for identifying evaporation using $\delta^{18}O$ (‰) and $\delta^{2}H$ (‰). In addition, poor results for $\delta^{13}C$ (‰) and pH are attributed to multiple, non-linear processes, and local processes affecting the C and H^+ concentrations in groundwater. Finally, Model 2a is selected for the EMMA, which only considers the chemical differences among the samples. This means that the evaporated Ca-HCO_3 end-member is representative of focused Mountain Front Recharge and shallow Mountain Block Recharge, as it is impossible to distinguish non-evaporated Ca-HCO_3. The composition of three eigenvectors (EG) of Model 2a is plotted in Figure 9 and defined by EG1, EG2, and EG3 in

Water Resources Research

10.1029/2023WR035719

Table 2

End-Member Mixing Analysis Results: Coefficient of Determination (R^2), Root-Mean-Squared Error (RMSE), Slope (m), and Total Representative Variance (%) of Major Solutes (mol/L), pH, and Stable $\delta^{18}O$, $\delta^{2}H$, and $\delta^{13}C$ Between Measured and Estimated Concentrations for a Subset of Models

	Variables																													
	Ca			Na			Mg			K			Cl			Alk			SO_4			pH[a]			$\delta^{18}O$			$\delta^{2}H$			$\delta^{13}C$			
Model	*m*	RMSE	R^2	*m*	RMSE	R^2	*m*	RMSE	R^2	*m*	RMSE	R^2	*m*	RMSE	R^2	*m*	RMSE	R^2	*m*	RMSE	R^2	*m*	RMSE	R^2	*m*	RMSE	R^2	*m*	RMSE	R^2	*m*	RMSE	R^2	Variance (%)
1	0.7	0.7	0.4	0.7	2.4	0.8	0.7	0.2	0.8	0.7	0.03	0.7	0.2	1.8	0.1	0.5	1.9	0.6	0.9	0.3	0.8	0.1	0.1	0.2										82
2	0.7	0.5	0.7	0.7	1.8	0.9	0.7	0.2	0.9	0.8	0.02	0.8	0.9	0.6	0.9	0.6	1.7	0.7	1.2	0.4	0.8	0.1	0.1	0.2										82
2a	0.7	0.5	0.7	0.8	1.9	0.9	0.7	0.2	0.9	0.8	0.00	0.8	1	0.6	0.9	0.6	1.7	0.7	1.1	0.4	0.8													86
2b	0.8	0.5	0.7	0.8	1.6	0.9	0.8	0.2	0.9	0.8	0.00	0.8	0.9	0.6	0.9	0.6	1.7	0.7	1.1	0.4	0.8				0.4	1.4	0.4							80
2c	0.7	0.5	0.7	0.8	1.7	0.9	0.7	0.2	0.8	0.8	0.00	0.8	0.9	0.6	0.9	0.6	1.7	0.7	1.1	0.4	0.3							0.4	9.1	0.4				81
2d	0.6	0.6	0.7	0.8	1.7	0.9	0.6	0.3	0.8	0.6	0.00	0.6	0.8	0.6	0.9	0.5	1.8	0.7	1.0	0.3	0.8										0.4	5.5	0.1	79

[a]Statistics computed with μmol/L of H due to low H concentration (<0.001 mol/L) and output format of MIX printing values up to three significant digits.

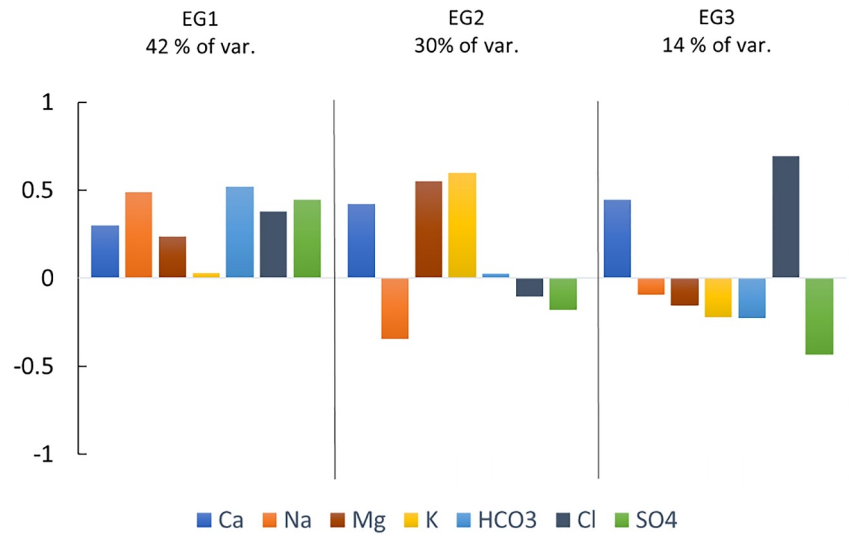

Figure 9. Contribution of eigenvectors 1, 2, and 3 to the total explained variance in the End-Member Mixing Analysis model 2a, and relative contribution of each species to each eigenvector. Positive and negative values indicate changes in sample concentration relative to the 0 value in the bivariate eigenvector space (Figure 10).

EG1–EG2 and EG2–EG3 spaces shown in Figure 10. The sign (±) of an EG is related to the eigenvectors space. Positive EG contributions in Figure 9 are related to changes in sample concentration plotted on the right side of the 0 value in the EG1–EG2 and EG2–EG3 (Figure 10). Negative contributions mean changes in samples concentration are on the left side of the 0 value.

The first eigenvector (EG1) explains 42% of the variance with similar positive contributions from all solutes except K (0.03) (Figure 9). Solutes with a higher positive contribution are Na (0.49), HCO_3 (0.52), SO_4 (0.45) and Cl (0.38). Therefore, EG1 seems to account for the main chemical evolution of groundwater and is likely associated with evapoconcentration, silicate weathering, calcite, and gypsum dissolution processes. Equal contribution in almost all solutes suggests evapoconcentration is the most representative process in EG1 (Figure 9).

The second eigenvector (EG2) explains 30% of the chemical variability and helps to distinguish among processes responsible for dissolved cations (Ca, Na, Mg, and K) evolution in groundwater. Three major processes identified based on EG2 contributions are biotite weathering (Section 3.1.1), responsible for increasing Mg and K concentrations (positive contribution in EG2, Figure 9), andesine weathering (Section 3.1.1) for increased dissolved Na (negative contribution in EG2, Figure 9), and CE for the positive contribution of Ca and the negative

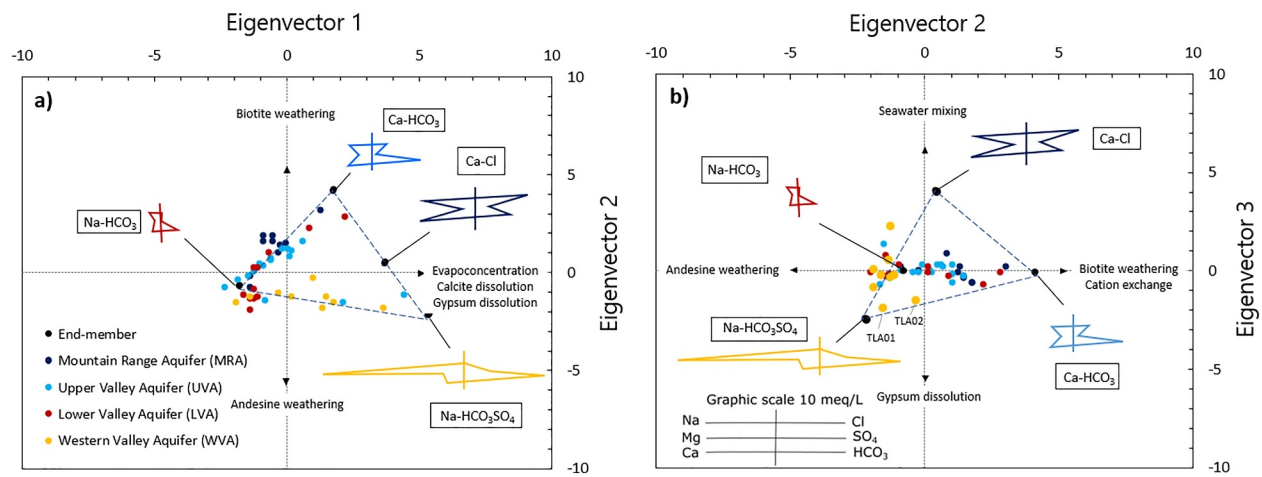

Figure 10. (a) Projection of solute concentrations to the first and second eigenvectors' space in End-Member Mixing Analysis model 2a. (b) Projection of solute concentrations to the second and third eigenvectors' space. Stiff diagrams represent the ion concentrations of end-members.

contribution of dissolved Na. Although calcite dissolution could also explain higher Ca concentration in EG2, a higher contribution of HCO_3 would be expected.

The third eigenvector (EG3) explains 14% of the groundwater chemical variability, and Cl (0.69) and Ca (0.44) are positively contributing to this EG while SO_4 contribution (−0.43) is negative (Figure 9). We attribute the Cl increase to mixing freshwater and seawater. The positive Ca contribution in EG3 instead of Na is related to selection of the Ca-Cl end-member. This end-member is the only sample of this groundwater type and by far has the highest dissolved Cl. Negative SO_4 contribution is attributed to gypsum dissolution even though Ca contribution is positive. We attribute this contradiction to the strong influence of the Ca-Cl end-member. The positioning of non-seawater mixing samples (TLA01 and TLA02) with the highest dissolved SO_4 and Na in Figure 10 agrees with the gypsum dissolution and andesine weathering.

Based on these and Section 3.1.1 results, the main processes driving Ca-HCO_3 groundwater type (representative of focused Mountain Front Recharge and shallow Mountain Block Recharge) are evapoconcentration, biotite weathering, CE, and calcite and gypsum dissolution (Figures 10a and 10b). Andesine and biotite weathering are the main processes influencing Na-HCO_3 groundwater indicative of Mountain Block Recharge (Figures 10a and 10b). The WVA groundwater is represented by the Na-HCO_3SO_4 groundwater type and is mainly affected by evapoconcentration, calcite dissolution, gypsum dissolution, and andesine weathering. Finally, the Ca-Cl groundwater type from this same region represents processes driven by evapoconcentration, calcite dissolution, gypsum dissolution, and seawater mixing. These results support the processes identified for each Mountain System Recharge process.

3.3.2. Improving EMMA by Considering Chemical Reactions

To further improve EMMA, the main geochemical processes affecting each eigenvector were considered in four EMMA models (B, C, D, E, and F; Table 3). These models aim to reduce the non-conservative behavior of solutes and improve model performance. The model performance was evaluated using RMSE and R^2 instead of the total explained variance. The total explained variance is only useful when comparing models with the same number of components. Chemical reactions are represented by conservative **u** components and reported in Table 3. To add a reaction to a **u** component, one new solute must be added with the new reaction (Pelizardi et al., 2017). Among all reactions only andesine and CE share the same solutes. Ca and Na solutes were considered for the **u**_andesine component due to its importance in the Lower and Western Valley Aquifers chemistry while CE was not included.

Highly satisfactory results are obtained by incorporating chemical reactions into EMMA instead of chemical solutes, as indicated by improved R^2 and RMSE statistics (Tables 2 and 4, and Figure S4 in Supporting Information S1). Model F has the best results with $R^2 = 0.9$, $0.1 \leq \text{RMSE} \leq 1.3$, and slopes between 0.8 and 1.1. As the number of components is equal to the number of end-members (i.e., three), 100% of the variance is explained by the model. These results further validate the proposed processes driving the groundwater chemistry in Section 3.1.1. These results agree with Pelizardi et al. (2017) where they compared the results of a synthetic model using simple solutes versus conservative components. Their results show that using conservative components instead of simple solutes decreases the objective functions as species affected by chemical reactions usually contribute to a higher percentage of the variance.

3.4. Quantifying Mountain Block Recharge and Focused Mountain Front Recharge Contributions to the Valley Aquifer System Using MIX

Relative contribution of each groundwater chemical facie to groundwater composition in each well was computed by running MIX 100 times for the EMMA model F. These proportions were attributed to focused Mountain Front Recharge and Mountain Block Recharge processes, given the characteristic chemical signature of each process inferred from Sections 3.1 and 3.2. We selected the top 5 models with the smallest differences between the measured and estimated concentrations to account for the uncertainty of estimated proportions. These results are reported in Table S8 for each well, and model averages are summarized in Figure 11. One of the most important results is the high proportion of deep Mountain Block Recharge recharging the Upper and Lower Valley Aquifers. Deep Mountain Block Recharge represents 47 ± 3% of the UVA, 53 ± 5% of the LVA, and 31 ± 4% of the WVA. The high percentage of deep Mountain Block Recharge in the UVA wells supports the hypothesis of a mixing zone in the unconfined and confined aquifers (Figure 9). Additionally, groundwater commonly used for irritation in the Central Valley causes this type of mixing. The Mountain Block Recharge proportion increases up to an

Table 3
Chemical Reactions Along With the Reacting Species and Conservative Components of Each Model

	Chemical reactions	Components
A	No chemical reactions	Na, Ca, Mg, K, Cl, SO_4, and alkalinity
B	Andesine dissolution (Equation 7)	$\mathbf{U}_{Andesine} = Ca - 0.7Na$
		Mg, K, Cl, SO_4, and alkalinity
C	Andesine dissolution (Equation 7)	$\mathbf{U}_{Andesine} = Ca - 0.7Na$
	Biotite dissolution (Equation 9)	$\mathbf{U}_{Biotite} = Mg - 3K$
		Cl, SO_4, and alkalinity
D	Andesine dissolution (Equation 7)	$\mathbf{U}_{And.–Gyp.} = Ca - 0.7Na - SO_4$
	Gypsum dissolution (Equation 11)	Mg, K, Cl, and alkalinity
E	Andesine dissolution (Equation 7)	$\mathbf{U}_{And.–Gyp.} = Ca - 0.7Na - SO_4$
	Biotite dissolution (Equation 9)	$\mathbf{U}_{Biotite} = Mg - 3K$
	Gypsum dissolution (Equation 11)	Cl and alkalinity
F	Andesine dissolution (Equation 7)	$\mathbf{U}_{And.–Gyp.–calc.} = Ca - 0.7Na - CO_3 - SO_4$
	Biotite dissolution (Equation 9)	$\mathbf{U}_{Biotite} = Mg - 3K$
	Gypsum dissolution (Equation 11)	Cl
	Calcite dissolution (Equation 5)	

average of 70% in the LVA when the Na-HCO_3SO_4 groundwater type is also considered. The focused Mountain Front Recharge and shallow Mountain Block Recharge account for 29 ± 1% of the UVA, 17 ± 1% of the LVA, and 17 ± 3% of the WVA.

The focused Mountain Front Recharge and shallow Mountain Block Recharge contribution decreases with increasing well depth and distance from the mountain front. These results are consistent with longer flow paths between the Lower and Western Valley Aquifers wells and the Sierra Nevada. As expected, the WVA has a higher influence from seawater mixing (average mixing proportion of 32 ± 6%). Higher Mountain Block Recharge contribution suggests greater connectivity between the Sierra Nevada and the sedimentary basin groundwater. These results agree with the recent studies highlighting the greater role of Mountain Block Recharge in valley aquifer recharge compared to focused Mountain Front Recharge (Aishlin & McNamara, 2011; Manning & Solomon, 2003; Markovich et al., 2019; Meixner et al., 2016) and can be used to better constrain future groundwater models for climate change assessment.

3.5. Future Work

Although environmental tracers and mixing calculations indicate higher fraction of deep Mountain Block Recharge in the valley aquifer, quantifying the magnitude of each Mountain System Recharge pathway remains highly uncertain (Manning & Solomon, 2005). The application of mixing ratios to determine recharge rates

Table 4
End-Member Mixing Analysis Results: Coefficient of Determination (R^2), Root-Mean-Squared Error (RMSE), and Slope (m) of Major Solutes, pH and Stable $\delta^{18}O$, δ^2H, and $\delta^{13}C$ Between Measured and Estimated Concentrations for Models B to F

	Variables																				
	Cl			Alkalinity			SO_4			Mg			K			U-Andesine			U-Biotite		
Model	R^2	RMSE	m	R^2	RMSE	m	R^2	RMSE	m	R^2	RMSE	m	R^2	RMSE	m	R^2	RMSE	m	R^2	RMSE	m
B	0.8	0.9	0.6	0.6	2.0	0.5	0.7	0.4	0.7	0.8	0.2	0.7	0.5	0.04	0.4	0.8	1.3	0.7			
C	0.6	0.2	0.6	0.6	1.9	0.7	0.6	0.5	1.0							0.6	3.0	0.2	0.6	0.3	0.4
D	0.7	1.5	0.4	0.9	0.7	1.0				0.5	0.3	0.6	0.7	0.03	0.5	0.9	0.9	1.0			
E	0.9	0.7	1.2	0.6	2.0	0.5										0.9	1.1	0.9	0.8	0.2	0.7
F	0.9	0.7	1.1													0.9	1.3	0.8	0.9	0.1	0.9

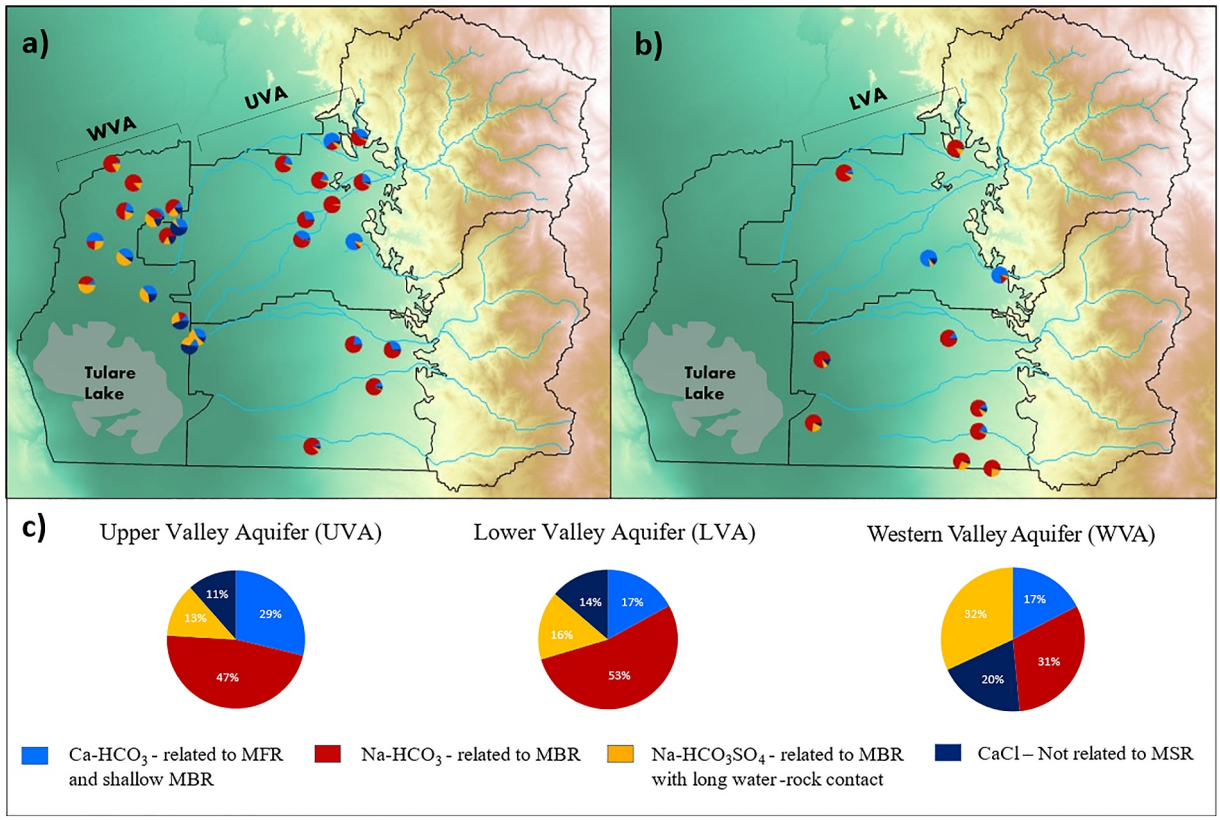

Figure 11. Mixing ratios of each sample in the (a) Upper Valley and Western Valley Aquifers, and (b) the Lower Valley Aquifer. (c) Average mixing ratios for each groundwater region. MFR, Mountain Front Recharge; MBR, Mountain Block Recharge; MSR, Mountain System Recharge.

requires an independent method for estimating total recharge (e.g., Ajami et al., 2012). Moreover, utilizing water balance approaches based on remote sensing data to estimate Mountain System Recharge poses significant challenges, particularly in highly managed mountain-valley aquifer systems with conjunctive use for irrigation. Factors contributing to this uncertainty include limited borehole logs and chemistry data in the mountain area, lack of accurate estimates of groundwater withdrawals in the basin (Brookfield et al., 2024), uncertainties in meteorological forcing (Schreiner-McGraw & Ajami, 2020, 2022) and groundwater storage estimates from the Gravity Recovery and Climate Experiment (GRACE) given its footprint (200,000 km^2) and errors in other terrestrial storage components estimates (Famiglietti et al., 2011). Recent integration of Global Positioning System displacements data with GRACE, reservoir and snow water equivalent data provides an overall Mountain Block Recharge estimate of 5 km^3/year in the Central Valley. However, this approach is unable to distinguish the contribution of focused Mountain Front Recharge from that of shallow versus deep Mountain Block Recharge (Argus et al., 2022). The next logical step is to combine information from nonreactive tracers, isotopes, and reactive solutes using particle tracking and reactive transport models integrated with the coupled surface-subsurface flow model for the joint evaluation of recharge rate estimates from multiple types of observations. Such a model-data fusion framework will improve mechanistic understanding of complex mountain-valley aquifer systems (L. Li et al., 2021).

4. Conclusions

We identified major hydrogeochemical processes responsible for the regional groundwater chemistry of the Sierra Nevada and northern Tulare Basin to understand Mountain System Recharge pathways. These pathways include diffuse and focused MAR, focused Mountain Front Recharge, and shallow and deep Mountain Block Recharge. The main sources of Mountain System Recharge are rain and snowmelt that, via direct infiltration through soil or surface water bodies, influence mountain-valley groundwater chemistry. Groundwater isogeochemistry data distinguishes three recharge end-members in the valley groundwater that

are influenced by hydrologic processes of mountain watersheds. Focused Mountain Front Recharge is associated with the evaporated Ca-HCO_3 groundwater type, and evapoconcentration, CE, biotite weathering, and calcite dissolution influence its composition. Shallow Mountain Block Recharge is mainly associated with the non-evaporated Ca-HCO_3 groundwater type, and CE, biotite weathering, and calcite dissolution affect its chemistry. The main source of shallow Mountain Block Recharge is snowmelt infiltration during the peak snowmelt. Focused Mountain Front Recharge and shallow Mountain Block Recharge, recharge the first 100 m of the upper aquifer. Deep Mountain Block Recharge is recharged during the peak of snowmelt and is mainly associated with Na-HCO_3 and Na-HCO_3SO_4 groundwater type that are influenced by andesine weathering and calcite and gypsum dissolution. This groundwater type has an apparent age of up to 40k years, and at some locations influenced by focused MAR highlighting the importance of surface water bodies recharging deep valley groundwater.

EMMA and MIX analysis revealed the spatial distribution of each recharge process associated with the major hydrogeochemical processes in groundwater. Considering four end-members in EMMA produced satisfactory results explaining 86% of the chemical variance. Considering water-rock reactions using conservative chemical components, significantly improved the model performance. These results highlight the importance of chemical reactions in EMMA and MIX analysis in cases where identifying conservative solutes is challenging. Mixing ratios show that 31%–53% of the groundwater system is recharged by Mountain Block Recharge originating from the Sierra Nevada. The high percentage of Mountain Block Recharge contribution indicates greater connectivity between the Sierra Nevada and the valley aquifer than previously thought (Meixner et al., 2016). These findings have important implications for groundwater resource availability under climate change due to projected changes in the Sierra Nevada snowpack.

This study highlights the importance of jointly analyzing groundwater chemistry with isotopes via a multi-tool approach to understand the main factors controlling groundwater and identify the main recharge processes. To our knowledge, this is the first comprehensive assessment of Mountain Block Recharge processes in the Sierra Nevada demonstrating the role of mountain aquifers and deep flow paths in recharging Central Valley. Similar studies in other mountain ranges with similar bedrock, and geological characteristics will improve the understanding of Mountain System Recharge processes, leading to sustainable groundwater management.

Conflict of Interest

The authors declare no conflicts of interest relevant to this study.

Data Availability Statement

Data sets for this research are available in Supporting Information S1, and all of them are also available at Armengol et al. (2024). The EMMA and MIX code is open source and available on https://idaea.csic.es/software/mix/.

Acknowledgments
This research has been supported by the National Science Foundation CAREER award (No. 1944161), and the USDA multistate fund (No. CA-R-ENS-5146-RR). We acknowledge USGS GAMA Program for providing the data set. We thank Flavia Pelizardi for guidance in constructing the conservative components and for comments on the manuscript.

References

Aishlin, P., & McNamara, J. P. (2011). Bedrock infiltration and mountain block recharge accounting using chloride mass balance. *Hydrological Processes*, *25*(12), 1934–1948. https://doi.org/10.1002/hyp.7950

Ajami, H., Meixner, T., Dominguez, F., Hogan, J., & Maddock, T., III. (2012). Seasonalizing mountain system recharge in semi-arid basins-climate change impacts. *Groundwater*, *50*(4), 585–597. https://doi.org/10.1111/j.1745-6584.2011.00881.x

Ajami, H., Troch, P. A., Maddock, T., III., Meixner, T., & Eastoe, C. (2011). Quantifying mountain block recharge by means of catchment-scale storage-discharge relationships. *Water Resources Research*, *47*(4), W04504. https://doi.org/10.1029/2010WR009598

Alam, S., Gebremichael, M., Li, R., Dozier, J., & Lettenmaier, D. P. (2019). Climate change impacts on groundwater storage in the Central Valley, California. *Climatic Change*, *157*(3), 387–406. https://doi.org/10.1007/s10584-019-02585-5

Appelo, C. A. J., & Postma, D. (2005). *Geochemistry, groundwater and pollution*. CRC Press.

Argus, D. F., Martens, H. R., Borsa, A. A., Knappe, E., Wiese, D. N., Alam, S., et al. (2022). Subsurface water flux in California's Central Valley and its source watershed from space geodesy. *Geophysical Research Letters*, *49*(22), e2022GL099583. https://doi.org/10.1029/2022GL099583

Armengol, S., Ajami, H., Acero, J., O'Sickman, J., & Ortega, L. (2024). Isogeochemical characterization of mountain system recharge processes in the Sierra Nevada, California [Dataset]. *Dryad*. https://doi.org/10.5061/dryad.0cfxpnw9t

Bales, R. C., Molotch, N. P., Painter, T. H., Dettinger, M. D., Rice, R., & Dozier, J. (2006). Mountain hydrology of the western United States. *Water Resources Research*, *42*(8), W08432. https://doi.org/10.1029/2005WR004387

Barnett, T. P., Adam, J. C., & Lettenmaier, D. P. (2005). Potential impacts of a warming climate on water availability in snow-dominated regions. *Nature*, *438*(7066), 303–309. https://doi.org/10.1038/nature04141

Barthold, F. K., Tyralla, C., Schneider, K., Vaché, K. B., Frede, H. G., & Breuer, L. (2011). How many tracers do we need for end member mixing analysis (EMMA)? A sensitivity analysis. *Water Resources Research*, *47*(8), W08519. https://doi.org/10.1029/2011WR010604

Bazuhair, A. S., & Wood, W. W. (1996). Chloride mass-balance method for estimating ground water recharge in arid areas: Examples from western Saudi Arabia. *Journal of Hydrology*, *186*(1–4), 153–159. https://doi.org/10.1016/S0022-1694(96)03028-4

Bennett, G. L. V., Fram, M. S., & Johnson, T. D. (2017). Groundwater-quality data in the Tulare shallow aquifer study unit, (2014–2015): Results from the California GAMA Priority Basin Project. US Geological Survey Data Release. https://doi.org/10.5066/F7BP00W8

Berghuijs, W. R., Woods, R. A., & Hrachowitz, M. (2014). A precipitation shift from snow towards rain leads to a decrease in streamflow. *Nature Climate Change*, *4*(7), 583–586. https://doi.org/10.1038/nclimate2246

Boiano, D. M., Weeks, D. P., & Hemry, T. (2005). *Sequoia and Kings Canyon National Parks, California: Water resources information and issues overview report*. Technical Report NPS/NRWRD/NRTR 2005/333. National Park Service.

Bresciani, E., Cranswick, R. H., Banks, E. W., Batlle-Aguilar, J., Cook, P. G., & Batelaan, O. (2018). Using hydraulic head, chloride and electrical conductivity data to distinguish between mountain-front and mountain-block recharge to basin aquifers. *Hydrology and Earth System Sciences*, *22*(2), 1629–1648. https://doi.org/10.5194/hess-22-1629-2018

Brookfield, A. E., Zipper, S., Kendall, A. D., Ajami, H., & Deines, J. M. (2024). Estimating groundwater pumping for irrigation: A method comparison. *Groundwater*, *62*(1), 15–33. https://doi.org/10.1111/gwat.13336

Carrera, J., Vázquez-Suñé, E., Castillo, O., & Sánchez-Vila, X. (2004). A methodology to compute mixing ratios with uncertain end-members. *Water Resources Research*, *40*(12), W12101. https://doi.org/10.1029/2003WR002263

Christophersen, N., & Hooper, R. P. (1992). Multivariate analysis of stream water chemical data: The use of principal components analysis for the end-member mixing problem. *Water Resources Research*, *28*(1), 99–107. https://doi.org/10.1029/91WR02518

Clow, D. W., Mast, M. A., Bullen, T. D., & Turk, J. T. (1997). Strontium 87/strontium 86 as a tracer of mineral weathering reactions and calcium sources in an alpine/subalpine watershed, Loch Vale, Colorado. *Water Resources Research*, *33*(6), 1335–1351. https://doi.org/10.1029/97WR00856

Clow, D. W., Mast, M. A., & Campbell, D. H. (1996). Controls on surface water chemistry in the upper Merced River basin, Yosemite National Park, California. *Hydrological Processes*, *10*(5), 727–746. https://doi.org/10.1002/(SICI)1099-1085(199605)10:5<727::AID-HYP316>3.0.CO;2-D

Coes, A. L., Pool, D. R., Stonestrom, D. A., Constantz, J., Ferre, T., & Leake, S. A. (2007). Ephemeral-stream channel and basin-floor infiltration and recharge in the Sierra Vista subwatershed of the Upper San Pedro Basin, southeastern Arizona (pp. 253–311). US Geological Survey Professional Paper.

Craig, H. (1961). Isotopic variations in meteoric waters. *Science*, *133*(3465), 1702–1703. https://doi.org/10.1126/science.133.3465.1702

Daly, C., Neilson, R., & Phillips, D. L. (1994). A statistical-topographic model for mapping climatological precipitation over mountainous terrain. *Journal of Applied Meteorology*, *33*(2), 140–158. https://doi.org/10.1175/1520-0450(1994)033<0140:astmfm>2.0.co;2

Davis, G. H., Green, J. H., Olmsted, F. H., & Brown, D. W. (1959). *Ground-water conditions and storage capacity in the San Joaquin Valley California (No 1469)*. US Government Printing Office.

De Vries, J. J., & Simmers, I. (2002). Groundwater recharge: An overview of processes and challenges. *Hydrogeology Journal*, *10*(1), 5–17. https://doi.org/10.1007/s10040-001-0171-7

Diepenbrock, A. (1933). Mount Poso oil field. *California Oil Fields*, *19*(2), 4–35.

Diffenbaugh, N. S., Swain, D. L., & Touma, D. (2015). Anthropogenic warming has increased drought risk in California. *Proceedings of the National Academy of Sciences*, *112*(13), 3931–3936. https://doi.org/10.1073/pnas.1422385112

Elnashar, A., Wang, L., Wu, B., Zhu, W., & Zeng, H. (2020). Synthesis of global actual evapotranspiration from 1982 to 2019. *Earth System Science Data Discussions*, *13*(2), 1–42. https://doi.org/10.5194/essd-13-447-2021

Famiglietti, J. S., Lo, M., Ho, S. L., Bethune, J., Anderson, K. J., Syed, T. H., et al. (2011). Satellites measure recent rates of groundwater depletion in California's Central Valley. *Geophysical Research Letters*, *38*(3), L03403. https://doi.org/10.1029/2010GL046442

Faunt, C. C., Belitz, K., & Hanson, R. T. (2010). Development of a three-dimensional model of sedimentary texture in valley-fill deposits of Central Valley, California, USA. *Hydrogeology Journal*, *18*(3), 625–649. https://doi.org/10.1007/s10040-009-0539-7

Faunt, C. C., Sneed, M., Traum, J., & Brandt, J. T. (2016). Water availability and land subsidence in the Central Valley, California, USA. *Hydrogeology Journal*, *24*(3), 675–684. https://doi.org/10.1007/s10040-015-1339-x

Feth, J. H. F., Robertson, C. E., & Polzer, W. L. (1964). *Sources of mineral constituents in water from granitic rocks, Sierra Nevada, California and Nevada*. US Government Printing Office.

Flint, A. L., Flint, L. E., Hevesi, J. A., & Blainey, J. B. (2004). Fundamental concepts of recharge in the desert southwest: A regional modeling perspective. In *Groundwater recharge in a desert environment: The southwestern United States* (Vol. 9, pp. 159–184). American Geophysical Union. https://doi.org/10.1029/009wsa10

Friedman, I., Smith, G. I., Gleason, J. D., Warden, A., & Harris, J. M. (1992). Stable isotope composition of waters in southeastern California 1. Modern precipitation. *Journal of Geophysical Research*, *97*(D5), 5795–5812. https://doi.org/10.1029/92JD00184

Frink, J. W., & Kues, H. A. (1954). Corcoran clay—A Pleistocene lacustrine deposit in San Joaquin Valley, California. *AAPG Bulletin*, *38*(11), 2357–2371. https://doi.org/10.1306/5CEAE0A0-16BB-11D7-8645000102C1865D

Frisbee, M. D., Phillips, F. M., Campbell, A. R., Liu, F., & Sanchez, S. A. (2011). Streamflow generation in a large, alpine watershed in the southern Rocky Mountains of Colorado: Is streamflow generation simply the aggregation of hillslope runoff responses? *Water Resources Research*, *47*(6), W06512. https://doi.org/10.1029/2010WR009391

Frisbee, M. D., Tolley, D. G., & Wilson, J. L. (2017). Field estimates of groundwater circulation depths in two mountainous watersheds in the western US and the effect of deep circulation on solute concentrations in streamflow. *Water Resources Research*, *53*(4), 2693–2715. https://doi.org/10.1002/2016WR019553

Fujii, R., & Swain, W. C. (1995). *Areal distribution of selected trace elements, salinity, and major ions in shallow ground water, Tulare Basin, southern San Joaquin Valley, California* (Vol. 95), No. 4048. US Department of the Interior, US Geological Survey.

Garrels, R. M., & Mackenzie, F. T. (1967). Origin of the chemical composition of springs and lakes. In *Equilibrium concepts in natural water systems*, *Advances in Chemistry Series* (Vol. 67, pp. 222–242). American Chemical Society. https://doi.org/10.1021/ba-1967-0067.ch010

Gleeson, T., & Manning, A. H. (2008). Regional groundwater flow in mountainous terrain: Three-dimensional simulations of topographic and hydrogeologic controls. *Water Resources Research*, *44*(10), W10403. https://doi.org/10.1029/2008WR006848

Goodrich, D. C., Williams, D. G., Unkrich, C. L., Hogan, J. F., Scott, R. L., Hultine, K. R., et al. (2004). Comparison of methods to estimate ephemeral channel recharge, Walnut Gulch, San Pedro River basin, Arizona. In *Groundwater recharge in a desert environment: The southwestern United States* (Vol. 9, pp. 77–99). https://doi.org/10.1029/009WSA06

Goyetche, T., Luquot, L., Carrera, J., Martínez-Pérez, L., & Folch, A. (2022). Identification and quantification of chemical reactions in a coastal aquifer to assess submarine groundwater discharge composition. *Science of the Total Environment*, *838*, 155978. https://doi.org/10.1016/j.scitotenv.2022.155978

Guan, H., Hutson, J., Ding, Z., Love, A., Simmons, C. T., & Deng, Z. (2013). Principal component analysis of watershed hydrochemical response to forest clearance and its usefulness for chloride mass balance applications. *Water Resources Research*, *49*(7), 4362–4378. https://doi.org/10.1002/wrcr.20357

Hilton, G. S., McClelland, E. J., Klausing, R. L., & Kunkel, F. (1963). Geology hydrology, and quality of water in the Terra Bella-Lost Hills area, San Joaquin Valley, California. USGS Open-File Report, 6347 (p. 158).

Hooper, R. P. (2003). Diagnostic tools for mixing models of stream water chemistry. *Water Resources Research*, *39*(3), 1055. https://doi.org/10.1029/2002WR001528

Hooper, R. P., Christophersen, N., & Peters, N. E. (1990). Modelling streamwater chemistry as a mixture of soilwater end-members—An application to the Panola Mountain catchment, Georgia, USA. *Journal of Hydrology*, *116*(1–4), 321–343. https://doi.org/10.1016/0022-1694(90)90131-G

Hoots, H. W., Bear, T. L., & Kleinpell, W. D. (1954). *Geological summary of the San Joaquin Valley, California*. Division of Mines.

Huth, A. K., Leydecker, A., Sickman, J. O., & Bales, R. C. (2004). A two-component hydrograph separation for three high-elevation catchments in the Sierra Nevada, California. *Hydrological Processes*, *18*(9), 1721–1733. https://doi.org/10.1002/hyp.1414

Inter-Agency Committee on Land Subsidence in the San Joaquin Valley. (1958). *Progress report on land-subsidence investigations in the San Joaquin Valley, California, through 1957*. The Committee.

Kang, S., Knight, R., & Goebel, M. (2022). Improved imaging of the large-scale structure of a groundwater system with airborne electromagnetic data. *Water Resources Research*, *58*(4), e2021WR031439. https://doi.org/10.1029/2021WR031439

Kendall, C., & Coplen, T. B. (2001). Distribution of oxygen-18 and deuterium in river waters across the United States. *Hydrological Processes*, *15*(7), 1363–1393. https://doi.org/10.1002/hyp.217

Klausing, R. L., & Lohman, K. E. (1964). Upper Pliocene marine strata on the east side of the San Joaquin Valley, California. US Geological Survey Professional Paper 475-D (pp. 14–17).

Lechler, A. R., & Niemi, N. A. (2012). The influence of snow sublimation on the isotopic composition of spring and surface waters in the southwestern United States: Implications for stable isotope–based paleoaltimetry and hydrologic studies. *Bulletin*, *124*(3–4), 318–334. https://doi.org/10.1130/B30467.1

Li, D., Wrzesien, M. L., Durand, M., Adam, J., & Lettenmaier, D. P. (2017). How much runoff originates as snow in the western United States, and how will that change in the future? *Geophysical Research Letters*, *44*(12), 6163–6172. https://doi.org/10.1002/2017GL073551

Li, L., Sullivan, P. L., Benettin, P., Cirpka, O. A., Bishop, K., Brantley, S. L., et al. (2021). Toward catchment hydro-biogeochemical theories. *Wiley Interdisciplinary Reviews: Water*, *8*(1), e1495. https://doi.org/10.1002/wat2.1495

Liu, Y., & Yamanaka, T. (2012). Tracing groundwater recharge sources in a mountain–plain transitional area using stable isotopes and hydrochemistry. *Journal of Hydrology*, *464*, 116–126. https://doi.org/10.1016/j.jhydrol.2012.06.053

Lofgren, B. E., & Klausing, R. L. (1969). *Land subsidence due to ground-water withdrawal, Tulare-Wasco area, California* (Vol. 437). US Government Printing Office. https://doi.org/10.3133/pp437B

Manning, A. H., & Solomon, D. K. (2003). Using noble gases to investigate mountain-front recharge. *Journal of Hydrology*, *275*(3–4), 194–207. https://doi.org/10.1016/S0022-1694(03)00043-X

Manning, A. H., & Solomon, D. K. (2005). An integrated environmental tracer approach to characterizing groundwater circulation in a mountain block. *Water Resources Research*, *41*(12), W12412. https://doi.org/10.1029/2005WR004178

Markovich, K. H., Manning, A. H., Condon, L. E., & McIntosh, J. C. (2019). Mountain-block recharge: A review of current understanding. *Water Resources Research*, *55*(11), 8278–8304. https://doi.org/10.1029/2019WR025676

Mast, M. A., Drever, J. I., & Baron, J. (1990). Chemical weathering in the Loch Vale watershed, Rocky Mountain National Park, Colorado. *Water Resources Research*, *26*(12), 2971–2978. https://doi.org/10.1029/WR026i012p02971

Maxey, G. B., & Eakin, T. E. (1949). Ground water in White River Valley, White Pine, Nye, and Lincoln Counties, Nevada.

Meade, R. H. (1967). *Petrology of sediments underlying areas of land subsidence in central California* (Vol. 497). US Government Printing Office.

Meixner, T., Manning, A. H., Stonestrom, D. A., Allen, D. M., Ajami, H., Blasch, K. W., et al. (2016). Implications of projected climate change for groundwater recharge in the western United States. *Journal of Hydrology*, *534*, 124–138. https://doi.org/10.1016/j.jhydrol.2015.12.027

Melack, J. M., Sadro, S., Sickman, J. O., & Dozier, J. (2020). *Lakes and watersheds in the Sierra Nevada of California: Responses to environmental change* (Vol. 5). University of California Press. https://doi.org/10.2307/j.ctv17hm9sr

Melack, J. M., Stoddard, J. L., & Ochs, C. A. (1985). Major ion chemistry and sensitivity to acid precipitation of Sierra Nevada lakes. *Water Resources Research*, *21*(1), 27–32. https://doi.org/10.1029/WR021i001p00027

Molins, S., Carrera, J., Ayora, C., & Saaltink, M. W. (2004). A formulation for decoupling components in reactive transport problems. *Water Resources Research*, *40*(10), W10301. https://doi.org/10.1029/2003WR002970

NADP. (2022). National Atmospheric Deposition Program. Retrieved from https://nadp.slh.wisc.edu/sites/ntn-ca75/

NLCD. (2019). National land cover dataset [Dataset]. Retrieved from https://www.usgs.gov/centers/eros/science/national-land-cover-database

NOAA. (2022). National water model CONUS retrospective dataset [Dataset]. Retrieved from https://registry.opendata.aws/nwm-archive

Park, W. H., & Weddle, J. R. (1959). Correlation study of southern San Joaquin Valley. Summary of operations. *California Oil Fields*, *45*(1), 33–34.

Parkhurst, D. L. (1997). Geochemical mole-balance modeling with uncertain data. *Water Resources Research*, *33*(8), 1957–1970. https://doi.org/10.1029/97WR01125

Parkhurst, D. L., & Appelo, C. A. J. (2013). Description of input and examples for PHREEQC version 3—A computer program for speciation, batch-reaction, one-dimensional transport, and inverse geochemical calculations. *US Geological Survey Techniques and Methods*, *6*(A43), 497.

Pelizardi, F., Bea, S. A., Carrera, J., & Vives, L. (2017). Identifying geochemical processes using End Member Mixing Analysis to decouple chemical components for mixing ratio calculations. *Journal of Hydrology*, *550*, 144–156. https://doi.org/10.1016/j.jhydrol.2017.04.010

Peng, T. R., Zhan, W. J., Tong, L. T., Chen, C. T., Liu, T. S., & Lu, W. C. (2018). Assessing the recharge process and importance of montane water to adjacent tectonic valley-plain groundwater using a ternary end-member mixing analysis based on isotopic and chemical tracers. *Hydrogeology Journal*, *26*(6), 2041–2055. https://doi.org/10.1007/s10040-018-1741-2

Rose, T. P., Davisson, M. L., & Criss, R. E. (1996). Isotope hydrology of voluminous cold springs in fractured rock from an active volcanic region, northeastern California. *Journal of Hydrology*, *179*(1–4), 207–236. https://doi.org/10.1016/0022-1694(95)02832-3

Rueedi, J., Purtschert, R., Beyerle, U., Alberich, C., & Kipfer, R. (2005). Estimating groundwater mixing ratios and their uncertainties using a statistical multi parameter approach. *Journal of Hydrology*, *305*(1–4), 1–14. https://doi.org/10.1016/j.jhydrol.2004.06.044

Scanlon, B. R., Faunt, C. C., Longuevergne, L., Reedy, R. C., Alley, W. M., McGuire, V. L., & McMahon, P. B. (2012). Groundwater depletion and sustainability of irrigation in the US High Plains and Central Valley. *Proceedings of the National Academy of Sciences*, *109*(24), 9320–9325. https://doi.org/10.1073/pnas.1200311109

Scanlon, B. R., Reedy, R. C., Stonestrom, D. A., Prudic, D., & Dennehy, K. F. (2005). Impact of land use and land cover change on groundwater recharge and quality in the southwestern US. *Global Change Biology*, *11*(10), 1577–1593. https://doi.org/10.1111/j.1365-2486.2005.01026.x

Schreiner-McGraw, A. P., & Ajami, H. (2020). Impact of uncertainty in precipitation forcing data sets on the hydrologic budget of an integrated hydrologic model in mountainous terrain. *Water Resources Research*, *56*(12), e2020WR027639. https://doi.org/10.1029/2020WR027639

Schreiner-McGraw, A. P., & Ajami, H. (2022). Combined impacts of uncertainty in precipitation and air temperature on simulated mountain system recharge from an integrated hydrologic model. *Hydrology and Earth System Sciences*, *26*(4), 1145–1164. https://doi.org/10.5194/hess-26-1145-2022

Schreiner-McGraw, A. P., Ajami, H., & Vivoni, E. R. (2019). Extreme weather events and transmission losses in arid streams. *Environmental Research Letters*, *14*(8), 084002. https://doi.org/10.1088/1748-9326/ab2949

Seager, R., Ting, M., Held, I., Kushnir, Y., Lu, J., Vecchi, G., et al. (2007). Model projections of an imminent transition to a more arid climate in southwestern North America. *Science*, *316*(5828), 1181–1184. https://doi.org/10.1126/science.1139601

Shaw, G. D., Conklin, M. H., Nimz, G. J., & Liu, F. (2014). Groundwater and surface water flow to the Merced River, Yosemite Valley, California: 36Cl and cl-evidence. *Water Resources Research*, *50*(3), 1943–1959. https://doi.org/10.1002/2013WR014222

Sisson, T. W., & Moore, J. G. (1984). *Geology of Giant Forest-Lodgepole Area, Sequoia National Park, California*. US Department of the Interior, Geological Survey.

Thaw, M., GebreEgziabher, M., Villafañe-Pagán, J. Y., & Jasechko, S. (2022). Modern groundwater reaches deeper depths in heavily pumped aquifer systems. *Nature Communications*, *13*(1), 5263. https://doi.org/10.1038/s41467-022-32954-1

Tobin, B. W. (2013). Contributions of karst groundwater to water quality and quantity in a mountain river basin: The Kaweah River, Sequoia and Kings Canyon National Parks, California (Doctoral dissertation). Texas State University-San Marcos. ProQuest. Retrieved from https://www.proquest.com/docview/1490982883?pq-origsite=gscholar&fromopenview=true

Tobin, B. W., & Schwartz, B. F. (2012). Quantifying concentrated and diffuse recharge in two marble karst aquifers: Big Spring and Tufa Spring, Sequoia and Kings Canyon National Parks, California, USA. *Journal of Cave and Karst Studies*, *74*(2), 186–196. https://doi.org/10.4311/2011JCKS0210

Tobin, B. W., & Schwartz, B. F. (2016). Using periodic hydrologic and geochemical sampling with limited continuous monitoring to characterize remote karst aquifers in the Kaweah River Basin, California, USA. *Hydrological Processes*, *30*(19), 3361–3372. https://doi.org/10.1002/hyp.10859

Visser, A., Moran, J. E., Singleton, M. J., & Esser, B. K. (2018). Importance of river water recharge to the San Joaquin Valley groundwater system. *Hydrological Processes*, *32*(9), 1202–1213. https://doi.org/10.1002/hyp.11468

Viviroli, D., Kummu, M., Meybeck, M., Kallio, M., & Wada, Y. (2020). Increasing dependence of lowland populations on mountain water resources. *Nature Sustainability*, *3*(11), 917–928. https://doi.org/10.1038/s41893-020-0559-9

Wahi, A. K., Hogan, J. F., Ekwurzel, B., Baillie, M. N., & Eastoe, C. J. (2008). Geochemical quantification of semiarid mountain recharge. *Groundwater*, *46*(3), 414–425. https://doi.org/10.1111/j.1745-6584.2007.00413.x

Wahrhaftig, C., & Birman, J. H. (1965). The Quaternary of the Pacific mountain system in California. In *The Quaternary of the US* (pp. 299–340). Princeton University Press.

Welch, L. A., & Allen, D. M. (2012). Consistency of groundwater flow patterns in mountainous topography: Implications for valley bottom water replenishment and for defining groundwater flow boundaries. *Water Resources Research*, *48*(5), 5526. https://doi.org/10.1029/2011WR010901

White, A. F., Bullen, T. D., Vivit, D. V., Schulz, M. S., & Clow, D. W. (1999). The role of disseminated calcite in the chemical weathering of granitoid rocks. *Geochimica et Cosmochimica Acta*, *63*(13–14), 1939–1953. https://doi.org/10.1016/S0016-7037(99)00082-4

Williams, M. W., Brown, A. D., & Melack, J. M. (1993). Geochemical and hydrologic controls on the composition of surface water in a high-elevation basin, Sierra Nevada, California. *Limnology & Oceanography*, *38*(4), 775–797. https://doi.org/10.4319/lo.1993.38.4.0775

Williams, M. W., Kattelmann, R., & Melack, J. M. (1990). Groundwater contributions to the hydrochemistry of an alpine basin. In *Paper presented at International Association of Hydrological Sciences Conference, Lausanne, Switzerland.*

Wilson, J. L., & Guan, H. (2004). Mountain-block hydrology and mountain-front recharge. In *Groundwater recharge in a desert environment: The Southwestern United States* (Vol. 9, pp. 113–137). https://doi.org/10.1029/009WSA08

Xiao, M., Koppa, A., Mekonnen, Z., Pagán, B. R., Zhan, S., Cao, Q., et al. (2017). How much groundwater did California's Central Valley lose during the 2012–2016 drought? *Geophysical Research Letters*, *44*(10), 4872–4879. https://doi.org/10.1002/2017GL073333

Zhu, C., Winterle, J. R., & Love, E. I. (2003). Late Pleistocene and Holocene groundwater recharge from the chloride mass balance method and chlorine-36 data. *Water Resources Research*, *39*(7), 1182. https://doi.org/10.1029/2003WR001987

References From the Supporting Information

Aeschbach-Hertig, W., Peeters, F., Beyerle, U., & Kipfer, R. (2000). Palaeotemperature reconstruction from noble gases in ground water taking into account equilibration with entrapped air. *Nature*, *405*(6790), 1040–1044. https://doi.org/10.1038/35016542

Carothers, W. W., & Kharaka, Y. K. (1980). Stable carbon isotopes of HCO_3 in oil-field waters-Implications for the origin of CO_2. *Geochimica et Cosmochimica Acta*, *44*(2), 323–332. https://doi.org/10.1016/0016-7037(80)90140-4

Coetsiers, M., & Walraevens, K. (2009). A new correction model for ^{14}C ages in aquifers with complex geochemistry–Application to the Neogene Aquifer, Belgium. *Applied Geochemistry*, *24*(5), 768–776. https://doi.org/10.1016/j.apgeochem.2009.01.003

Jung, M., Wieser, M., von Oehsen, A., & Aeschbach-Hertig, W. (2013). Properties of the closed-system equilibration model for dissolved noble gases in groundwater. *Chemical Geology*, *339*, 291–300. https://doi.org/10.1016/j.chemgeo.2012.08.006

Leybourne, M. I., Clark, I. D., & Goodfellow, W. D. (2006). Stable isotope geochemistry of ground and surface waters associated with undisturbed massive sulfide deposits; constraints on origin of waters and water–rock reactions. *Chemical Geology*, *231*(4), 300–325. https://doi.org/10.1016/j.chemgeo.2006.02.004

McCallum, J. L., Dogramaci, S., Cook, P. G., Banks, E., Purtschert, R., Irvine, M., et al. (2018). Stochastic correction of carbon-14 activities: A Bayesian approach with argon-39 validation. *Journal of Hydrology*, *566*, 396–405. https://doi.org/10.1016/j.jhydrol.2018.08.047

Moran, J. E., Esser, B. K., Hillegonds, D., Holtz, M., Roberts, S. K., Singleton, M. J., & Visser, A. (2011). *California GAMA special study: Nitrate fate and transport in the Salinas Valley* (No. LLNL-TR-484186). Lawrence Livermore National Lab. (LLNL). https://doi.org/10.2172/1122241

Scheiber, L., Ayora, C., Vázquez-Suñé, E., Cendón, D. I., Soler, A., Custodio, E., & Baquero, J. C. (2015). Recent and old groundwater in the Niebla-Posadas regional aquifer (southern Spain): Implications for its management. *Journal of Hydrology*, *523*, 624–635. https://doi.org/10.1016/j.jhydrol.2015.01.076

Vogel, J. C. (1993). Variability of carbon isotope fractionation during photosynthesis. In *Stable isotopes and plant carbon-water relations* (pp. 29–46). Academic Press. https://doi.org/10.1016/B978-0-08-091801-3.50010-6

Whiticar, M. J., & Faber, E. (1986). Methane oxidation in sediment and water column environments—Isotope evidence. *Organic Geochemistry*, *10*(4–6), 759–768. https://doi.org/10.1016/S0146-6380(86)80013-4